Optimal Electromyogram Modeling and Processing During Active Contractions and Rest

by

Haopeng Wang

A Thesis

Submitted to the Faculty

of the

WORCESTER POLYTECHNIC INSTITUTE

in partial fulfillment of the requirements for the

Degree of Master of Science

in

Electrical and Computer Engineering

April 2019

APPROVED:

_____

Dr. Edward A. Clancy, Research Advisor

_____

Dr. Xinming Huang, Committee Member

_____

Dr. Moinuddin Bhuiyan, Committee Member

Abstract

The standard deviation of surface EMG (EMGσ) is often related to muscle force; the accuracy of EMGσ estimation is valuable for many application areas such as clinical biomechanics, prostheses control and sports medicine. Numerous researchers have developed methods to optimize EMGσ estimation. Whitening the EMG signal has been proved to improve the statistical efficiency of EMGσ estimation, but conventional linear whitening filters fail at low contraction level. An adaptive whitening filter was proposed by Clancy and Farry[14]. This technique has a better performance than prior whitening methods, however, the adaptive whitening filter needs to be calibrated each time electrodes are applied, which increase the complexity of the implementation. We designed a universal whitening filter which can omit most calibration steps for the adaptive whitening filter in future use. We used the ensemble mean of the power spectrum of 512 EMG recordings to form a general shape of a fixed whitening filter that can applied on any EMG signal. The test error on an EMG-torque task based on universal whitening over 512 subjects had a mean error of 4.80% maximum voluntary contraction (MVC) and standard deviation (std) of 2.03% MVC, compared with an original adaptive whitening filter error of 4.84±1.98% MVC.

Additionally, the rest contraction modeling hasn't received enough attention. Existing RMS estimates of EMGσ subtract noise in either the amplitude or power domain. These procedures have never been modeled analytically. We show that power domain noise subtraction is optimal. But rest contractions which are processed using power domain noise subtraction only estimate a zero-valued EMGσ approximately 50% of the time, which is undesirable in prosthesis-control. The prosthesis has a 50% possibility to slowly drift based on the current RMS estimator. We propose a new estimator to improve the zero-amplitude estimation probability during rest. We used 512 rest contraction recordings to validate the probability distribution of rest EMG signal showing that it only has 1.6% difference compared with Gaussian distribution. We also evaluated the percent of zero-valued EMGσ estimates using power domain noise subtraction and our new estimator, matching experimental findings to the theoretic predictions.

Acknowledgement

Foremost, I'm deeply thankful to my research advisor, Professor Edward A. Clancy, who introduced me to the biomedical field and make me realize how much we can contribute to human health as an electrical and computer engineering student. I really appreciate for his guidance, not only advising me in this particular project, but also helping me build an academic thinking pattern and understand the philosophy of research. I'm really looking forward to future collaboration with him in my Phd life.

I also want to thank my senior students Ziling and Jianan, and alumnus Dr. Chenyun Dai; they provided me a lot of help and instruction during this whole project.

And I need to thank my teammates, He Wang and Kiriaki J. Rajotte. We worked on different aspects in this project; the idea exchanging progress really provided me a new insight of the whole project.

Finally, I want to thank my parents, Shenwen Wang and Haiyan Feng. They provide me unconditional love and support during my master's study.

Table of content

Table of Figures

Table of tables

1. Introduction

1.1 Contributions to this project

This project has two stages, both of which were team project cooperated with two other graduate students at WPI, He Wang and Kiriaki J. Rajotte. The first stage is the universal whitening filter design. The second stage is the EMG rest contraction analysis. Both stages are under the supervision of Dr. Clancy. In the first stage, I calibrated the 512 EMG recordings to generate the coefficient matrix of universal whitening filter and compare the performance of our new universal whitening filter with the original subject-specific calibrated filter on an EMG-torque model. For the second stage, I followed the theoretical analysis of Dr. Clancy's mathematical description of EMG rest contractions, and experimentally demonstrate the modeling of probability density function and power spectrum of rest contraction EMG signal.

1.2 Main content of the thesis

This thesis contains two parts of study, both aimed at improving EMG modulation and standard deviation estimation. The first part of the thesis describes a new whitening technique that simplifies the adaptive whitening filter process and tested a new whitening technique on EMG-torque models which showed an identical performance with original adaptive whitening. The second part uses 512 rest contraction recordings to show that the probability distribution of rest contraction is very closely Gaussian distributed. Based on the Gaussian distribution, we formed a new RMS processor with a gain factor applied to the noise. I demonstrated that the new RMS processor can reject additional noise during rest contraction. All the studies in the thesis were performed off-line in MATLAB. One conference paper has been published and an appendix of rest contraction modeling was written by Dr. Clancy.

1.3 Electromyogram

Electromyogram (EMG) is a recording of the electrical activity produced by skeletal muscles. It presents the electrical potential generated by muscle cells whenever the cells are electrically or neurologically excited [23]. Skeletal muscles are connected to the skeleton to form part of the mechanical system which moves the limbs and other parts of the body. The whole muscle is comprised of (usually parallel) muscle fascicles. Figure 1.1 shows a detailed structure of skeletal muscle. A collection of muscle fibers form muscle fascicles. There are two types of muscle fibers: Type I which is also known as "slow-twitch" fibers and Type II known

as “fast-twitch” fibers. “Slow-twitch” fibers generate more ATP from aerobic metabolism and the contractions of “slow-twitch” fibers are slower and less forceful. On the contrary, “fast-twitch” fibers generate more ATP from glucose and provide faster and more forceful contractions.

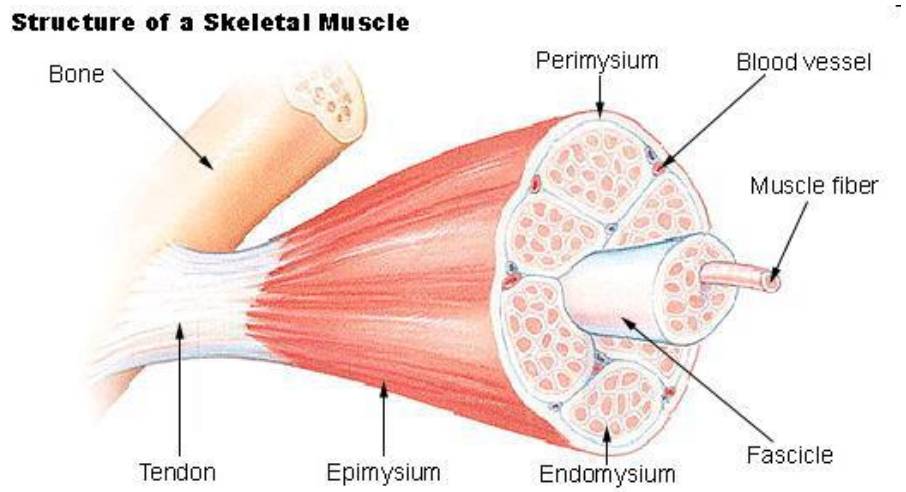

Figure 1.1 Detailed structure of skeletal muscle [2].

1.4 Muscle electrical activity generation

The first recorded muscle electrical activity and the term “electromyogram” was given in the 1890s [6]. Clinical electromyograms are commonly acquired by attaching electrodes to the muscles or skin surface. Recordings collected from the skin surface are referred to as surface EMG or sEMG [7]. sEMG is often comprised of frequencies under 600Hz [24], and sEMG could be modeled as amplitude-modulated with additive Gaussian noise [25]. We often use the standard deviation(EMGσ) of sEMG as EMG amplitude [26] and it contains valuable information. EMGσ is related to muscular effort, lower muscular effort means lower EMGσ and vice versa. The muscle force in overall muscle is regulated by two aspects: the number of active motor units and firing rate. It is observed that the standard deviation of the raw EMG signal is monotonically related to the number of the activated motor units and the rate of their activation. The definition of a motor unit is one motor nerve and all innervated muscle fibers (Figure 1.2 shows the structure of a motor unit). The muscle fibers in one motor unit are the same type. If the motor unit is activated, all the innervated muscle fibers contract, the muscle fibers follow the “all or nothing” rule.

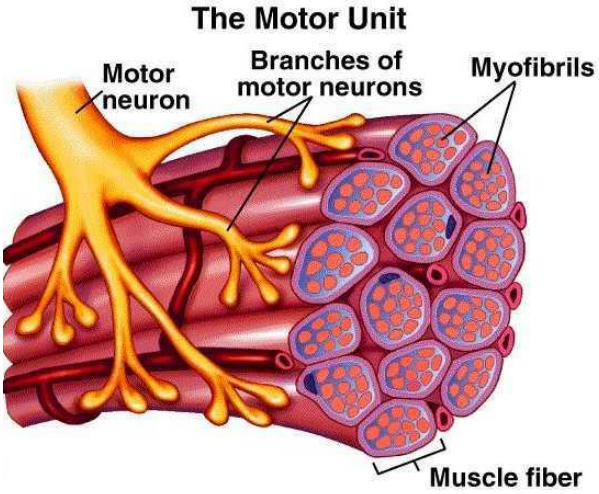

Figure 1.2 Structure of motor unit [3].

The electrical “action potential” recorded from a motor unit is the sum of voltages due to each muscle fiber. Figure 1.3 presents the typical transmembrane potential of a muscle cell. The rest potential is at around –70 mV. When muscle fibers are activated, the action potential peaks could reach to +30 mV. The duration of one action potential is usually 2–4 ms or longer [27]. During muscle contraction, the single motor unit will continuously generate similar shape action potentials. And, the shape of action potentials between different motor units are generally different. Figure 1.4 shows the model of one individual motor unit.

So, the EMG recording is the summation of the impulse responses generated by multiple active motor units. And since it’s the summation of multiple independent, rather identically shaped pulses, it could be modulated as Gaussian random process. A model for generation of the surface EMG signal is shown as Figure 1.5. An additive noise comes along with the EMG signal recording.

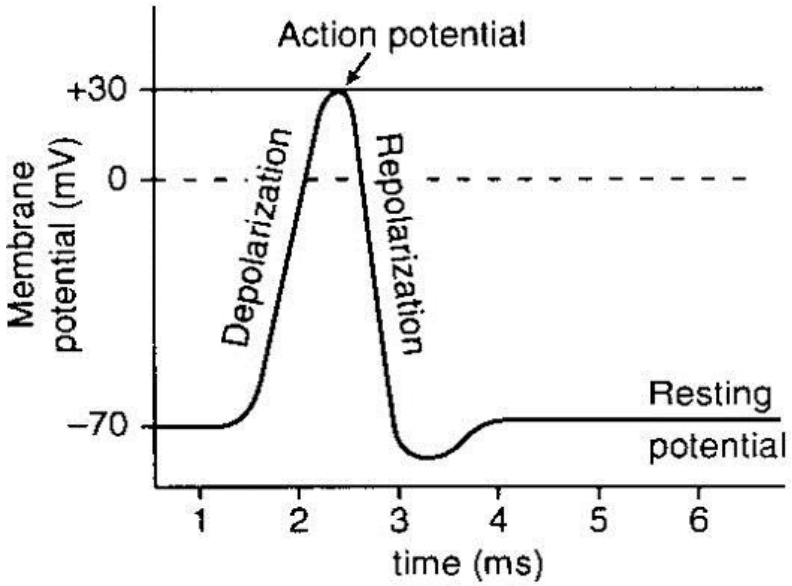

Figure 1.3 typical transmembrane potential of a muscle cell [4].

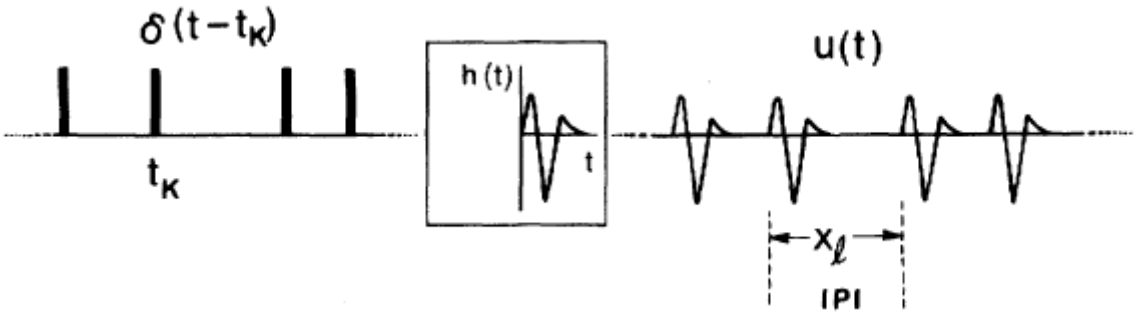

Figure 1.4 Schematic for the motor unit action potential train [5].

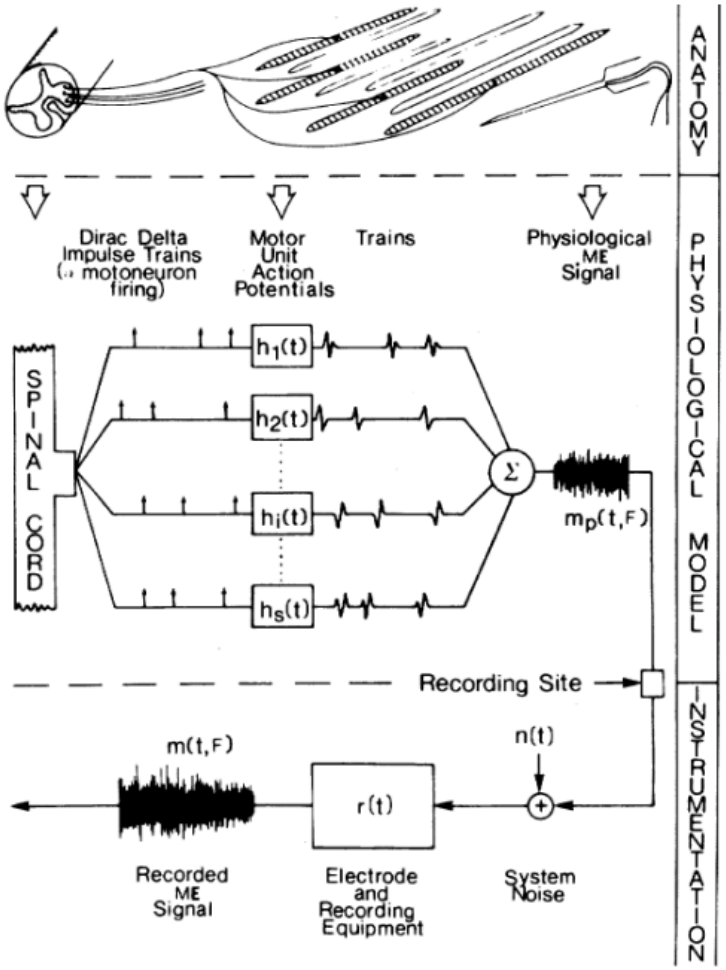

Figure 1.5 Complete engineering model of motor unit action potential [5].

1.5 EMGσ estimation

The recorded EMG from an electrode described from section 1.4 is also referred to as the raw EMG signal. Surface EMG collects a non-invasive measure of muscle activation and the raw EMG signal data used in this thesis are all from surface EMG.

After recording the raw EMG signal, we need to run through several signal processing steps to get an estimated EMGσ. EMGσ has been used in many fields and real-world applications, such as myoelectric prostheses control, ergonomics gait analysis and sports [28]. Plenty of studies have been developed to improve the estimation of EMGσ [14, 16, 29, 30]. (Figure 1.6 shows EMGσ estimation).

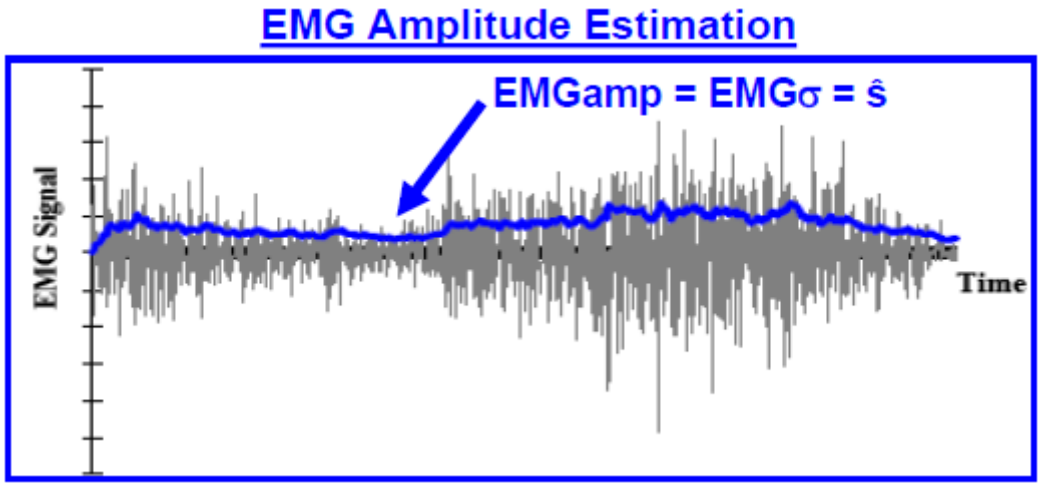

Figure 1.6 EMGσ estimation [9].

The two basic EMGσ estimators are: moving-average-root-mean-square (RMS) processor and moving-average-mean-absolute-value (MAMAV) processor. EMG can be modeled as an amplitude modulated zero-mean stochastic process as below:

$$m[n] = s[n] * v[n]$$

where $m[n]$ is raw EMG signal, $s[n]$ is EMGσ and $v[n]$ is a random noise process with unit variance. And the two estimators can be described as:

MARMS processor:

$$\hat{s}_{\mathrm{RMS}} = \sqrt{\frac{1}{L} * \sum_{k=n-L+1}^{n} m^2[k]}$$

MAMAV processor:

$$\hat{s}_{\mathrm{MAV}} = \frac{1}{L} * \sum_{k=n-L+1}^{n} |m[k]|$$

where L refers to window length.

The moving average in these two processors performs as low-pass filtering; the window length could be considered as cut-off frequency. A longer window means lower cut-off frequency which is suitable for slowly changing EMGσ. In contrast, a shorter window means higher cut-off frequency that could be used on rapidly changing EMGσ. So, the simple method

of EMGσ estimation can be considered as three steps described in Figure 1.7. For the MAMAV processor, we can skip the relinearization step because d=1 in the detection.

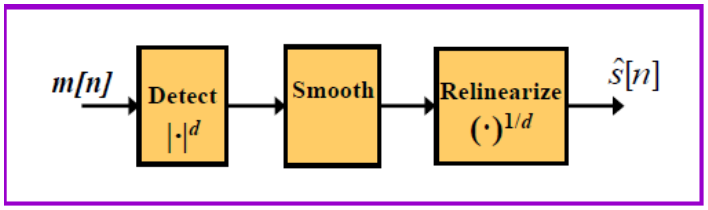

Figure 1.7 EMGσ estimator: 1. non-linear detection; 2. Low-pass filter (smoother) 3. Relinearize [10].

For a single site of EMG signal, several techniques have been proved to improve the estimation of EMGσ [14,16]. First, applying a high-pass filter prior to the RMS or MAV processor can help attenuate motion artifact noise. The cut-off frequency is often set up to 10-20 Hz because the power of motion artifacts is usually concentrated below 20 Hz. A higher cut-off frequency for the highpass filter might cause loss of useful EMG signal. Second, whitening the signal can increase the statistical bandwidth of EMG and reduce the variance of the EMGσ estimate at the same time. Different whitening techniques have been applied to improve estimation accuracy, such as reduced electrode spacing [12], digital filtering (off-line) [13], and analog filtering [13]. The whitening techniques have been widely used in EMGσ estimation, such as relating EMG-torque models. However, conventional whitening techniques might fail at low-level contractions. The adaptive whitening method [14] proposed by Clancy and Farry has overcome this issue. Figure1.8 shows a detailed process of optimal single site EMG amplitude estimation.

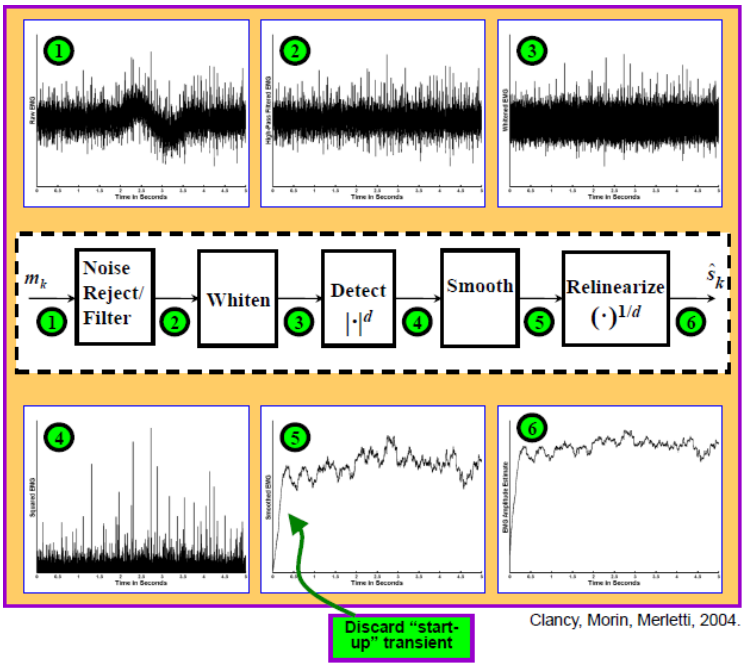

Figure 1.8: Optimal single site EMGσ estimation [11].

Beyond single site EMG recording optimized estimation, there are studies on multiple channel combinations of EMG signal [12, 13, 15, 16]. The combination of EMG signal recorded from different electrodes placed adjacent to each other can improve the signal-to-noise ratio. However, we need a gain normalization process to eliminate the gain difference between electrodes, so that each electrode is equally contributing to the recording. Research has shown that using several electrodes for measuring the EMG improves the accuracy of EMGσ estimation [16]. Overall, the multi-channel optimal EMGamp estimation has six stages: 1. Noise rejection/highpass filter; 2. Adaptive whitening; 3. Multiple Channel Combination and Gain Normalization; 4. Rectification and Demodulation; 5. Smoothing and 6. Relinearization (shown in Figure 1.9).

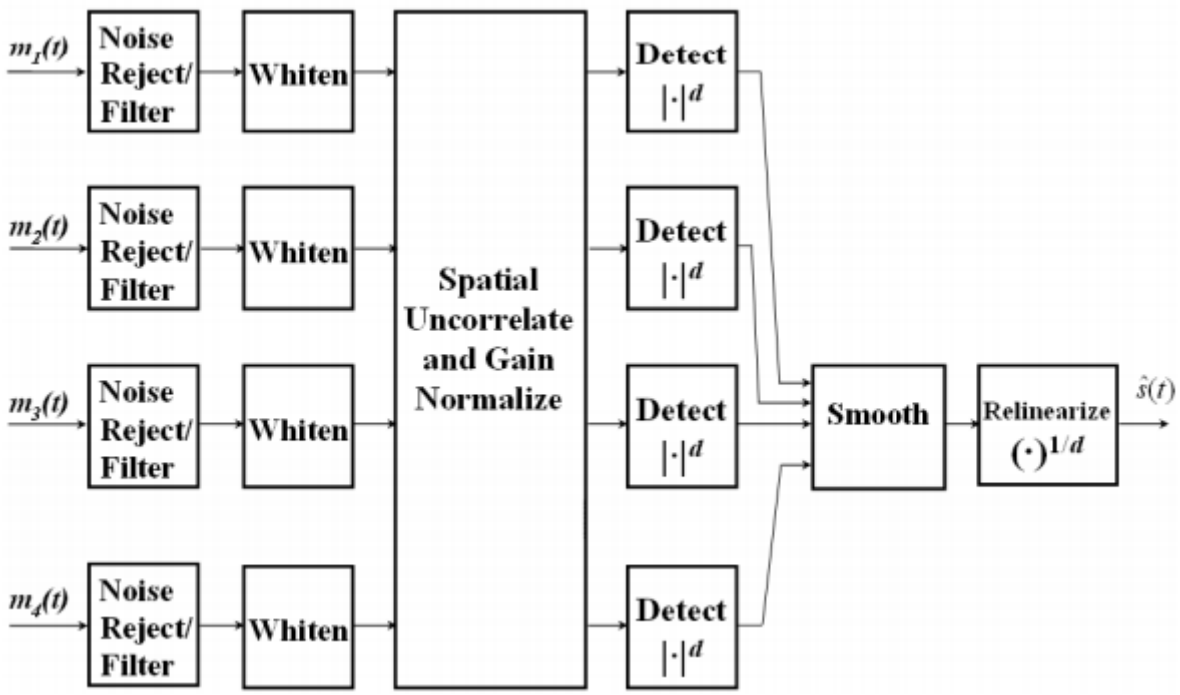

Figure 1.9 Six Stages Multi-Channel EMGσ Processor [17].

A precise EMGσ estimate could help improve EMG-torque modeling [21]. The goal of EMG-torque models is to simulate the natural relationship between the central nervous system (as evidenced in the surface EMG) and peripheral joints/muscles. The muscle tension is related to EMG. When muscle tension increases, EMG increases, but it's difficult to measure individual motor unit tension and tension in whole muscle. On the contrary, joint torque is easy to be measured or estimated accurately. So, developing an EMG-torque model can help interpret the EMG-force relation better. The general steps of relating EMG to torque is shown in Figure 1.10. Four surface electrodes are attached the muscles (biceps and triceps) to record the EMG signals as shown. The raw EMG signal is used to estimate EMGσ. The EMGσ

estimations for flexion and extension are decimated. The amplitude estimates are used as two inputs to a system identification algorithm to predict the joint torque.

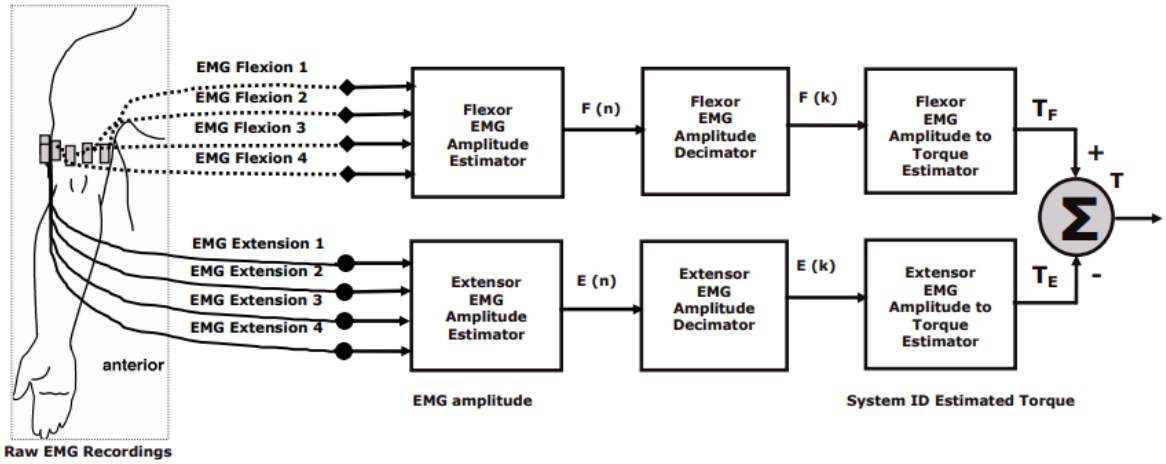

Figure 1.10 EMG-torque estimation model [18].

1.6 Experimental data

Experimental data were utilized from four prior experiments [14,19-21], combined to form a new data set containing 64 subjects in total. Those data re-use was approved and supervised by the WPI Institutional Review Board (WPI IRB). Each subject has 8 EMG channels, four elbow extension channels and four elbow flexion channels. Each channel has a corresponding rest contraction (0% MVC). All contractions were constant-posture [21]. Five second duration, constant-force contractions at 50% MVC extension, 50% MVC flexion and at rest were recorded, the data sampling frequency is 4096 Hz [21]. A total of 1024 raw EMG recordings (512 0% MVC recordings, 512 50% MVC extension or flexion recordings) are used for analysis in this thesis. The data were collected by eight separate electrodes attached to the skin surface of subjects. Four electrodes on biceps and four electrodes on triceps. The subjects were seated and strapped in the straight-back chair (Figure 1.11) by belts. The right shoulder was fixed by a belt and their arms are parallel with ground. The angle between their upper arm and forearm is 90^o, their right wrists were perpendicular to the floor and tightly cuffed to a load cell. The skin above biceps and triceps was disinfected by alcohol before attaching the electrodes. The electrodes were placed across the muscle group, in the midway between elbow and the midpoint of upper arm with elastic bandages. All contractions were constant-posture. Subjects warmed up before data collection. Separate extension and flexion MVCs were measured when subjects slowly increased their force to MVC and maintained constant for two seconds. The average load cell value was taken as the MVC. Then, 5-second,

constant-force contractions at 50% MVC extension and 50% MVC flexion and at rest were recorded. Three minutes rest was provided between each trial to avoid cumulative fatigue.

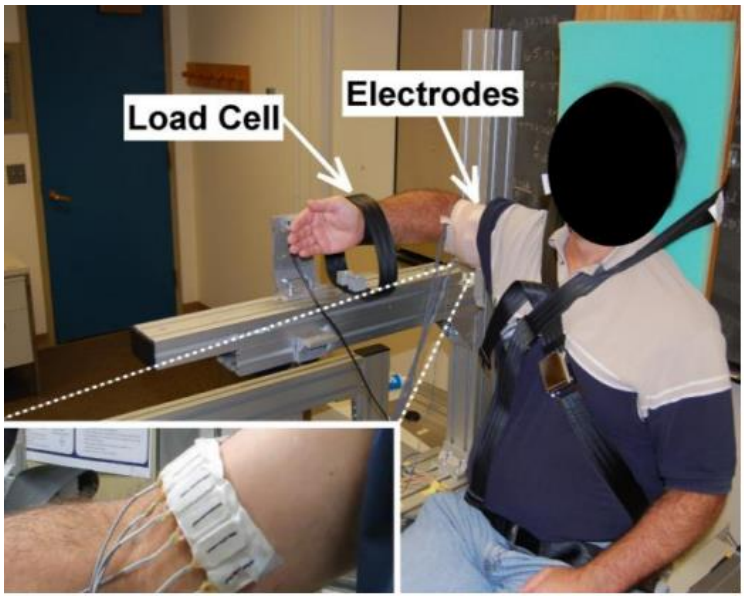

Figure 1.11 Subject posture and electrode placement [21].

2. Simplified adaptive whitening filter design

Whitening the surface electromyogram (EMG) has been proved to improve EMGσ estimation and minimize error in relating the surface EMG to elbow joint torque [14]. But conventional linear whitening filters can fail at low EMG amplitude levels. A three-stage adaptive whitening filter [14] was designed to overcome this problem.

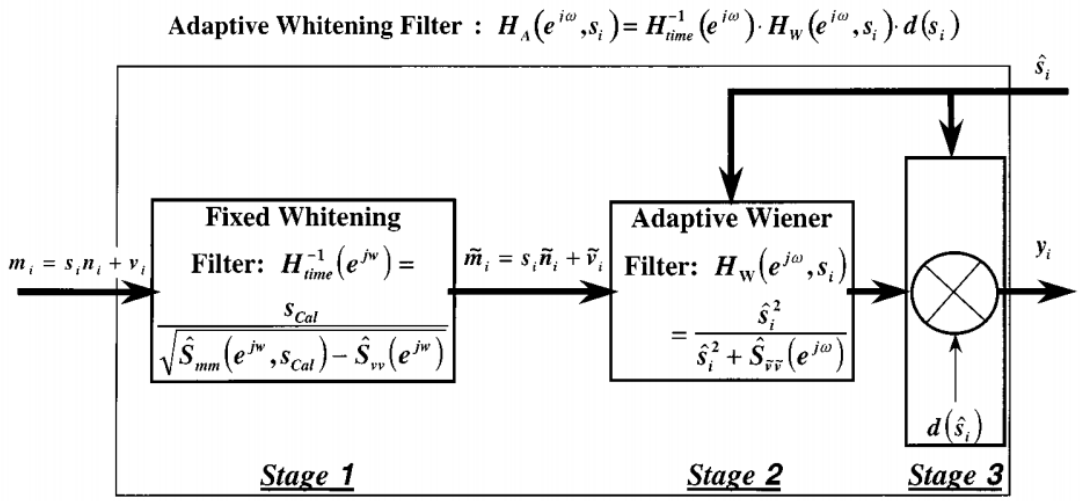

Figure. 2.1 Single site EMG adaptive whitening filter [14].

The first stage of the adaptive whitening filter is a fixed whitening filter that whitens the noise-free portion of the signal but also passes a filtered version of the additive noise at the same time. The second stage is an adaptive Wiener filter that attenuates the additive noise and estimates the noise-free whitened signal. The third stage applies an adaptive gain correction to preserve EMG amplitude scaling [14]. After adaptive whitening, the EMGσ is estimated in the conventional way: root-mean-square (RMS) processor or mean-absolute-value (MAV) processing.

The whole filter with three stages needs to be calibrated from two, constant-angle, constant-force contractions, one at a reference level [e.g. 50% maximum voluntary contraction (MVC)], and another one at 0% MVC (rest contraction). This whitening technique is not widely used mainly because the whiteners are calibrated to each subject, which makes the implementation more complex. Since the fixed whitening filter calibrated by different subjects has similar shapes, low gain at low frequencies and higher gain at high frequencies, we designed an “Universal” fixed whitening shape, and combined it with an adaptive noise canceller to form a new adaptive whitening process.

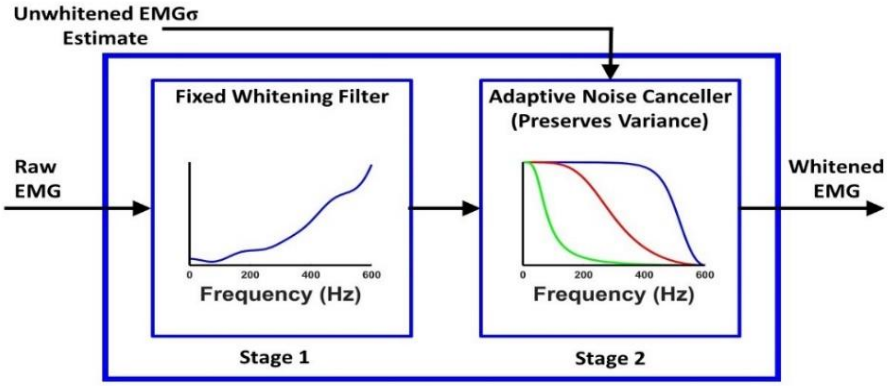

Figure 2.2 Two-stage adaptive whitening filter.

2.1 Universal fixed whitening filter calibration

We used a total of 512 recordings at each of 0% MVC and 50% MVC (64 subjects x 8 channels) to calibrate the fixed whitening filter. Each channel was individually processed. Because of the EMG gain or the force level differences between subjects, we need to normalize each recording to a same level of magnitude. We formed a normalization gain using the root mean square of 50% MVC:

$$Normalization\ gain = \frac{0.5}{\sqrt{\frac{\sum_1^N m_i^2}{N}}}$$

where m is the raw EMG signal.

And we multiplied this same gain by the 0% MVC recordings corresponding to the 50% MVC. After normalization, each recording was highpass filtered by a fifth-order Butterworth filter at 15 Hz cut-off frequency to remove the mean and attenuate motion artifacts. And the fixed whitening filter shape was derived from the inverse of the square root of power subtraction between 50%MVC and 0% MVC [14]. We have 512 sets of filter coefficients from which to form a universal whitening shape. We extracted power spectrum estimates from all 512 subjects, and computed the ensemble mean to create our new filter. We saved the filter coefficient in a matrix and use this filter shape as the first stage of adaptive whitening. Thus, we don't need to calibrate the fixed whitening filter for each recording in the future.

2.2 Testing the performance of universal whitening filter

We applied the new universal whitening filter to EMGσ estimation, and related EMG to force, using the test error as the indication of whitening performance. The data used in testing were described in section 1.6.

We tested it on 8 individual channels using a 15th order quadratic model. Coefficients were determined using least square via the Moore-Penrose inverse, with a tolerance of 0.0056 [21]. The original subject-specific whitening filter used two trials of EMG signal data for calibration and tested on the third trial. The mean error and the standard deviation over 512 subjects was 4.84±1.98% MVC, which set a baseline for our new technique testing. The new filter was evaluated on the EMG-force model in the similar way, producing an average ± std. dev. test error of 4.80±2.03% MVC which is similar to the performance of the subject-specific whitening filters.

	Test error mean	Test error std
Subject-specific whitening	4.84%	1.98%
Universal whitening	4.80%	2.03%

Table 2.1 Testing error of original and new whitening techniques

3. EMG signal model evaluation (PDF and PSD)

3.1 Probability density evaluation of 0% MVC and 50% MVC EMG signal

The probability density function (PDF) of the surface electromyogram (EMG) signal has been modeled with Gaussian and Laplacian distribution functions [22]. Knowing the probability density of the EMG signal could help us refine the EMGσ estimators. So, we used a total of 512 recordings each of 0% and 50% MVC (64 subjects x 8 electrodes/subject) to evaluate the probability density model of rest EMG and EMG from a constant force level.

The initial evaluation was applied on processed EMG signal without whitening. Each recording was sent through a fourth-order Butterworth highpass filter at 15-Hz cut-off frequency to remove the mean and attenuate motion artifacts. We then omitted first 500ms of data to remove start-up transients due to the filter.

Then we normalized the signal by subtracting the mean and dividing by the standard deviation of each recording to form a zero-mean, unit variance random process. And all the subjects are now in the same amplitude range so that we could take the ensemble average in later analysis. If $x[n]$ represents the signal after highpass filter and removed start-up transient, form a new signal vector $y[n]$ by normalization:

$$y[n] = \frac{x[n] - E(x[n])}{std(x[n])}$$

we can easily derive the mean and standard deviation of $y[n]$:

$$mean(y[n]) = E(y[n]) = \frac{E(x[n]) - E(E(x[n]))}{std(x[n])} = 0$$

and

$$std(y[n]) = \frac{std(x[n] - E(x[n]))}{std(x[n])} = 1$$

The normalization step is a linear operation, so it won't change the distribution type.

We created a histogram estimation with 501 bins equally distributed from -5 to 5 with an increment of 0.02 for each recording. The area of the histogram is normalized to 1 to force the Y-axis to display the probability.

After processing and creating PDF estimates for each recording, we have 1024 PDF estimations for 0% MVC trials and 50% MVC trials. The ensemble sample mean and standard deviation of the PDF from 512 0% MVC trials and 512 50% MVC trials gives us a general PDF estimation of rest EMG and 50% MVC EMG.

Each recording's probability distribution has zero-mean. The mean value of the ensemble sample average is obviously. We compared the ensemble average PDF with Gaussian and Laplacian distribution.

The ensemble sample mean and standard deviation through 512 0% MVC subjects and 512 50% MVC subjects are shown in Figure 3.1 and Figure 3.2 separately, along with ideal zero-mean, unit-variance Gaussian and Laplacian distributions.

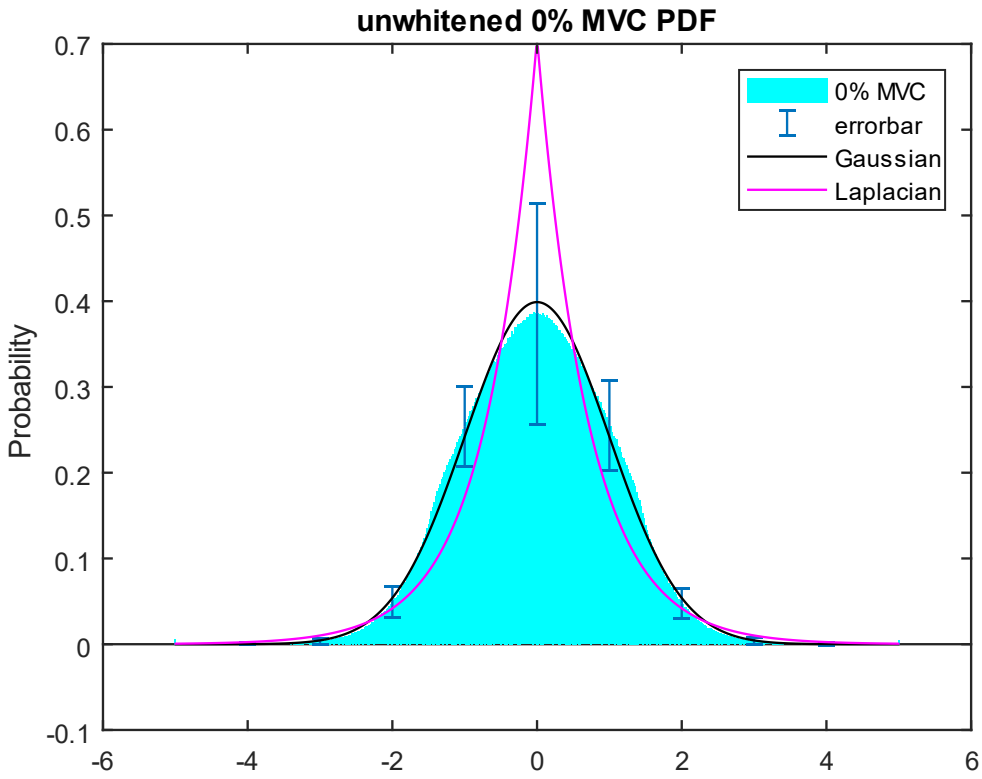

Figure 3.1 Ensemble average histogram estimate of unwhitened 0% MVC PDF (cyan), standard deviation between subjects (blue bar), ideal Gaussian distribution (black) and ideal Laplacian distribution (magenta).

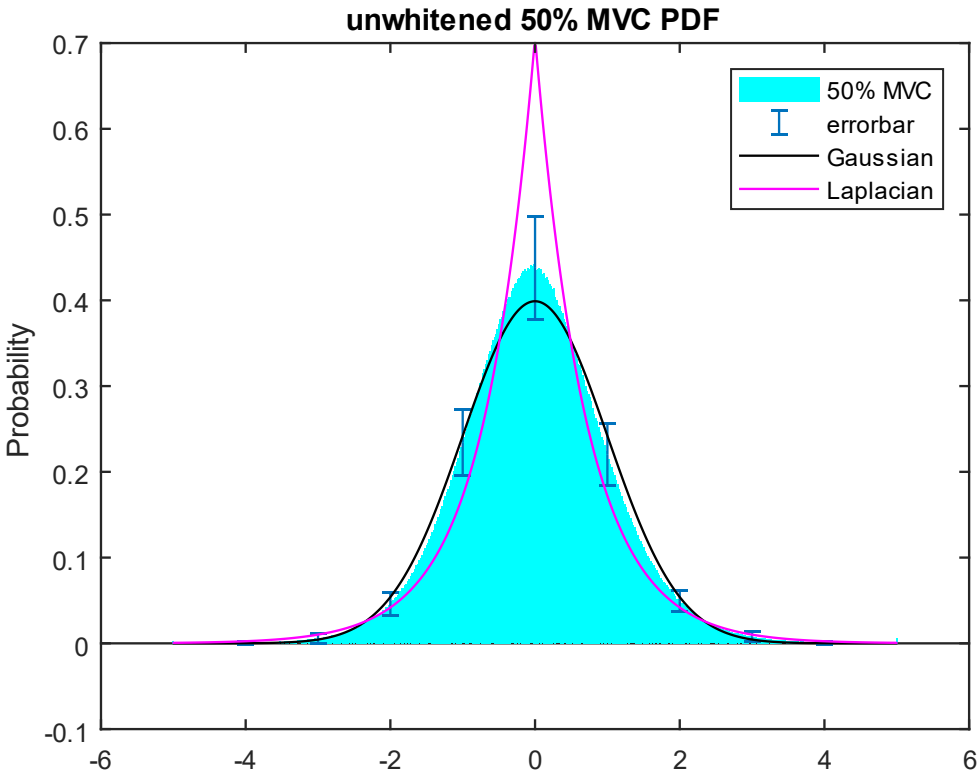

Figure 3.2. Ensemble average histogram estimate of unwhitened 50% MVC PDF (cyan), standard deviation between subjects (blue bar), ideal Gaussian distribution (black) and ideal Laplacian distribution (magnet).

For unwhitened signal, we calculate the absolute area difference between ensemble average versus a zero-mean unit-variance Gaussian distribution and Laplacian distribution to identify the similarity between EMG signal PDF and ideal distribution shape. EMG signal versus Gaussian difference was found to be 0.0514 for 0% MVC and 0.0764 for 50% MVC; and EMG signal versus a Laplacian density was found to be 0.3174 for 0% MVC and 0.2151 for 50% MVC.

Unwhitened signal	Gaussian	Laplacian
0% MVC	0.0514	0.3174
50% MVC	0.0764	0.2151

Table 3.1. The absolute area difference between unwhitened EMG signal versus Gaussian and Laplacian density.

The Gaussian and Laplacian distribution in above figures are all unit-variance, we can select different standard deviations to get a better fit for the probability distribution. We compared the absolute area differences between EMG signal PDF estimate with Gaussian distribution and Laplacian distribution with different stds. The standard deviation ranges from 0.5 to 2 with an increment of 0.05. Figure 3.3 and 3.4 show the absolute area differences versus standard deviation of ideal Gaussian and Laplacian distribution.

The minimum absolute area difference of 0% MVC is 0.0514 when comparing with Gaussian distribution of standard deviation = 1. The minimum absolute area difference of 50% MVC is 0.0534 when comparing with Gaussian distribution of standard deviation = 0.95.

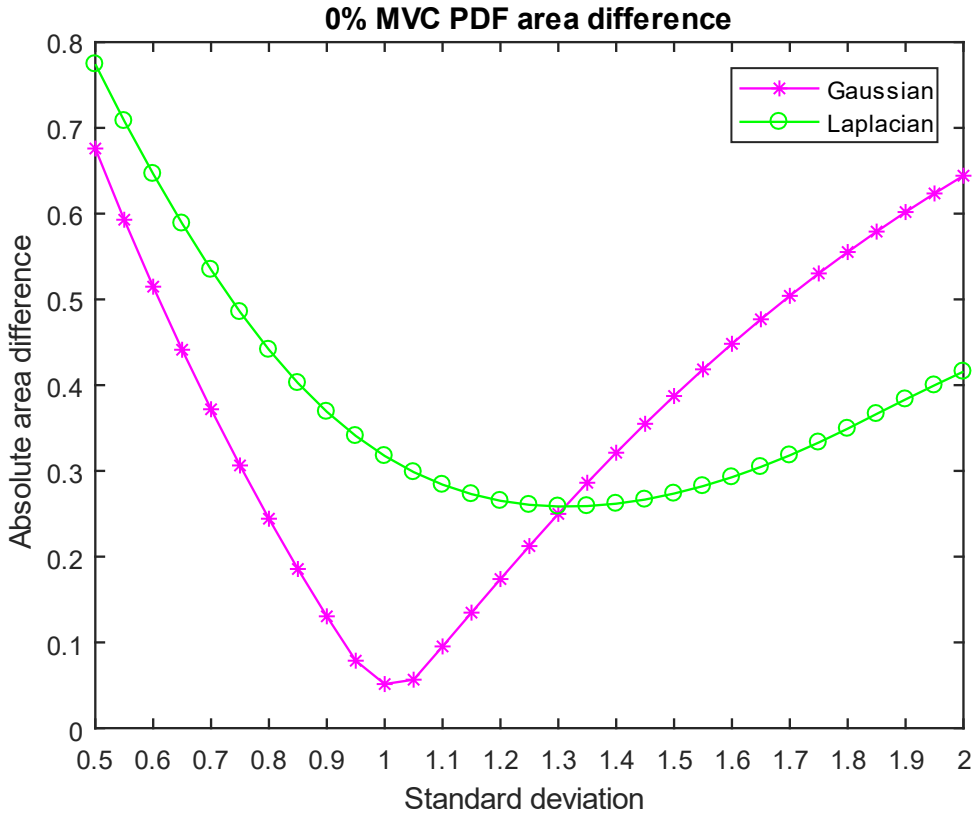

Figure 3.3 Absolute area difference versus standard deviation with both Gaussian and Laplacian (0% MVC unwhitened signal).

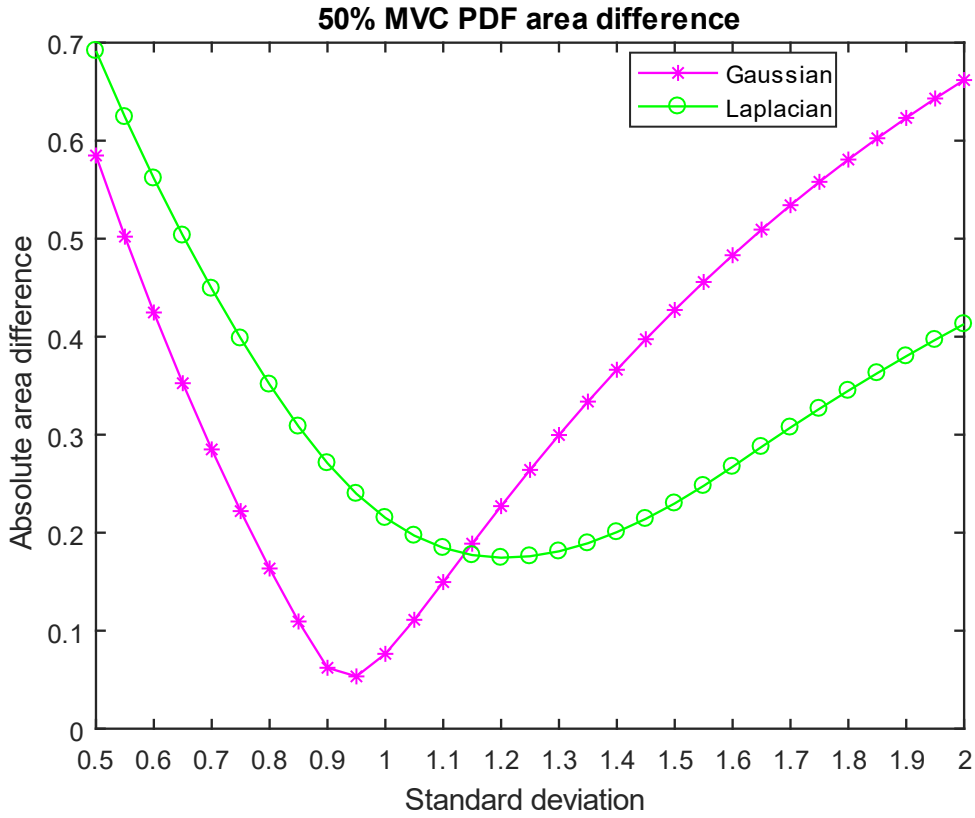

Figure 3.4 Absolute area difference versus standard deviation with both Gaussian and Laplacian (50% MVC unwhitened signal).

Based on the minimum absolute area difference of 0% MVC and 50% MVC, we can see Gaussian model is a better fit for both unwhitened 0% MVC and 50% MVC EMG signal. We provided the best fit of PDF estimate of 0% MVC and 50% MVC in Figure 3.5. Gaussian model for 0% MVC has a standard deviation of 1, and gaussian model for 50% MVC has a standard deviation of 0.95.

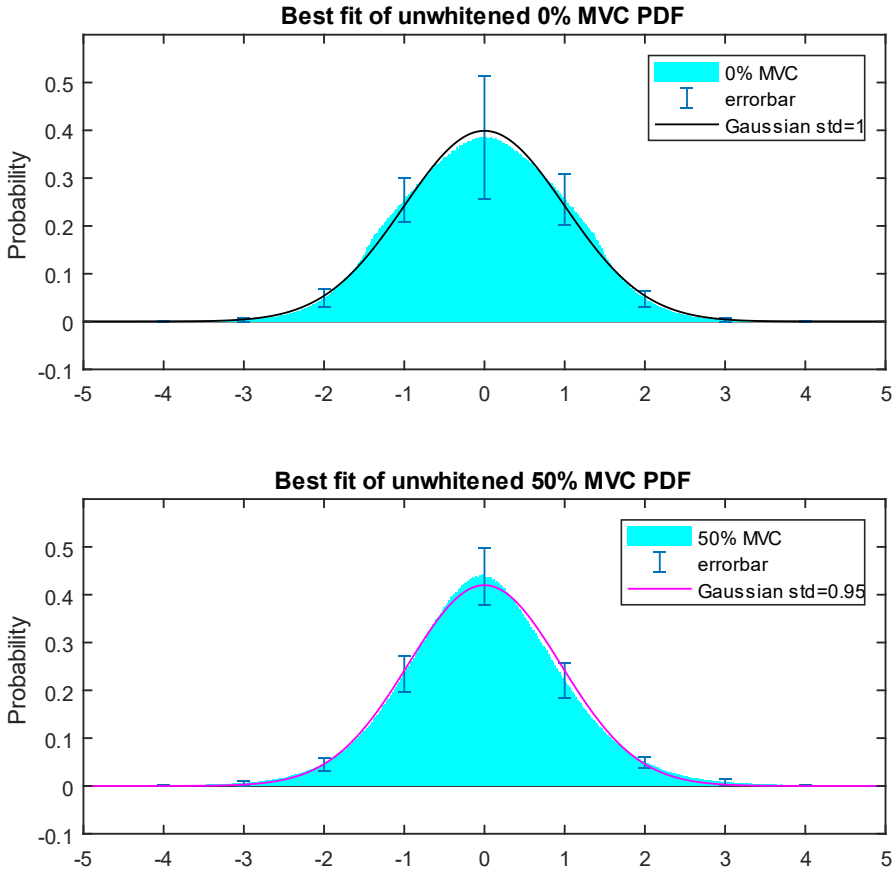

Figure 3.5 Best fit of unwhitened 0% MVC and 50% MVC PDF.

Then, we evaluate the PDF distribution of whitened 0% MVC and 50% MVC signals. Each recording was high passed by a fourth-order Butterworth filter at 15-Hz cut-off frequency to remove the mean and attenuate motion artifacts and then passed an adaptive whitening filter to temporally uncorrelate the signal and lower the variance. The adaptive whitening filter [14] was set to a band limit of 600 Hz. We omit the first 500 ms of data to remove start-up transients. We then normalized the signal with the same way of unwhitened signal analysis. Each recording is a zero-mean, unit variance random process. We created a histogram PDF estimation with 501 bins equally distributed from -5 to 5 with an increment of 0.02 for each recording. The area of the histogram is normalized to 1 to force the Y-axis to display the probability.

Then we created the plot of ensemble sample mean and standard deviation through 512 0% MVC trials and 512 50% MVC trials, along with ideal zero-mean, unit-variance Gaussian and Laplacian distributions (Figure 3.6 and Figure 3.7).

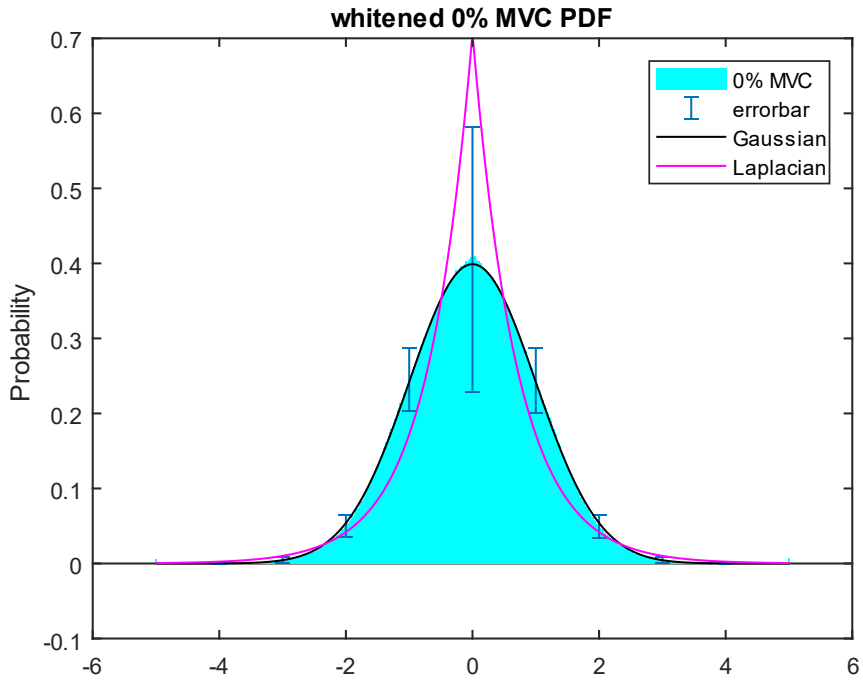

Figure 3.6 Ensemble average histogram estimate of whitened 0% MVC PDF (cyan), standard deviation between subjects (blue bar) ideal Gaussian distribution (black) and ideal Laplacian distribution (magenta).

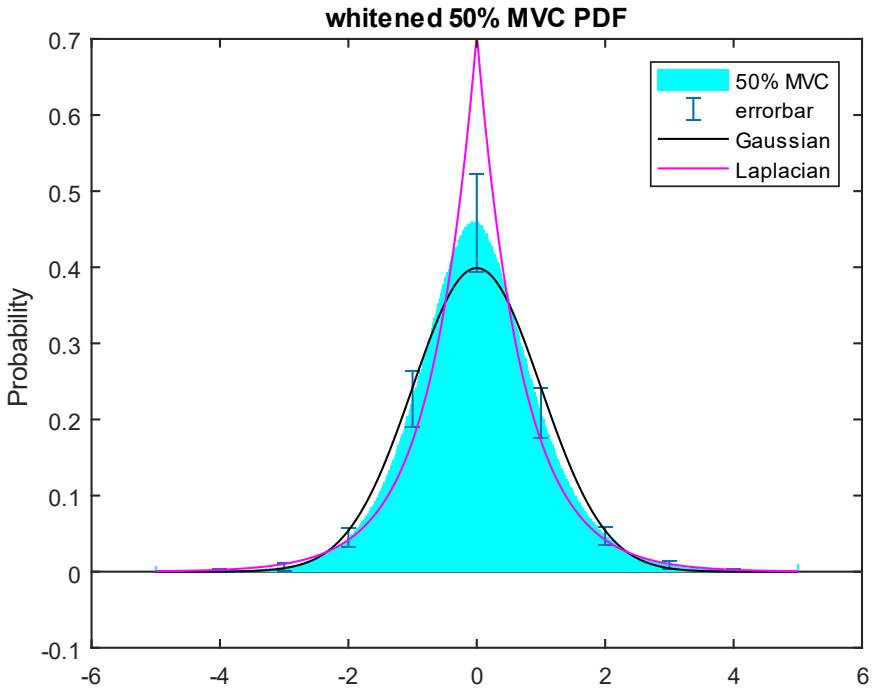

Figure 3.7 Ensemble average histogram estimate of whitened 50% MVC PDF (cyan), standard deviation between subjects (blue bar), ideal Gaussian distribution(black) and ideal Laplacian distribution(magenta).

For whitened signals, the absolute area difference between the ensemble average versus a Gaussian distribution was found to be 0.0160 for 0% MVC and 0.1141 for 50% MVC; and ensemble average versus a Laplacian distribution was found to be 0.2789 for 0% MVC and 0.1831 for 50% MVC.

Whitened signal	Gaussian	Laplacian
0% MVC	0.0160	0.2789
50% MVC	0.1141	0.1831

Table 3.2. The absolute area difference between whitened EMG signal versus Gaussian and Laplacian density.

The Gaussian and Laplacian distribution in above figures are all unit-variance, we can select different standard deviations to get a better fit for the probability distribution. We compared the absolute area differences between whitened EMG signal PDF estimate with Gaussian distribution and Laplacian distribution with different stds. The standard deviation ranges from 0.5 to 2 with an increment of 0.05. Figure 3.8 and 3.9 show the absolute area differences versus standard deviation of ideal Gaussian and Laplacian distribution.

The minimum absolute area difference of 0% MVC is 0.0160 when comparing with Gaussian distribution of standard deviation = 1. The minimum absolute area difference of 50% MVC is 0.0741 when comparing with Gaussian distribution of standard deviation = 0.90.

Both 0% MVC and 50% MVC have PDF estimates closer to ideal Gaussian and Laplacian distributions after whitening. Thus, if we modeled EMG signal as Gaussian or Laplacian distribution, whitening can improve the accuracy of EMGσ estimates.

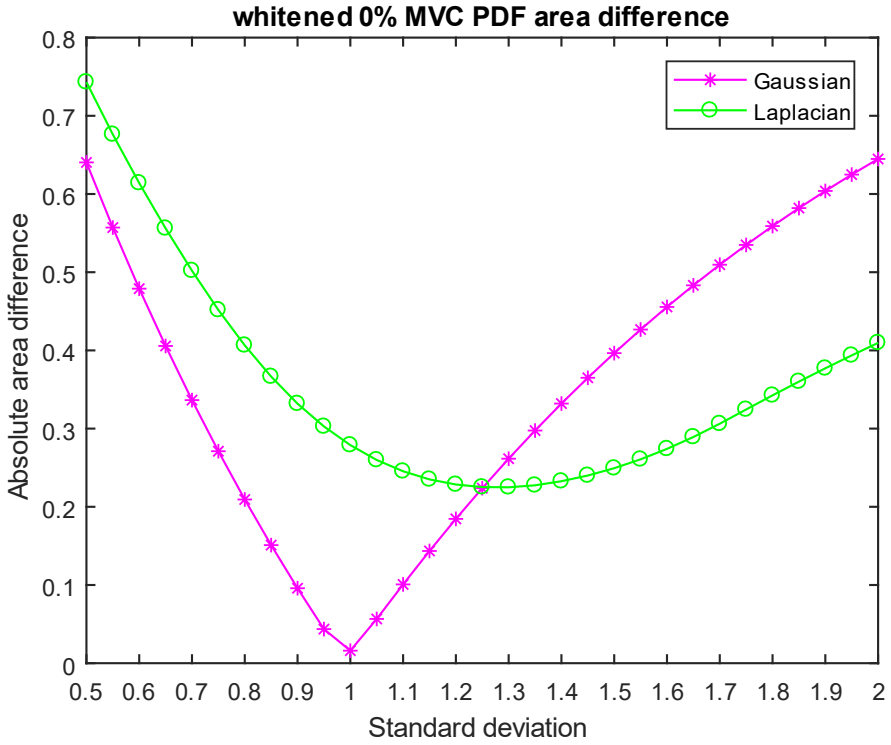

Figure 3.8 Absolute area difference versus standard deviation with both Gaussian and Laplacian (0% MVC whitened signal).

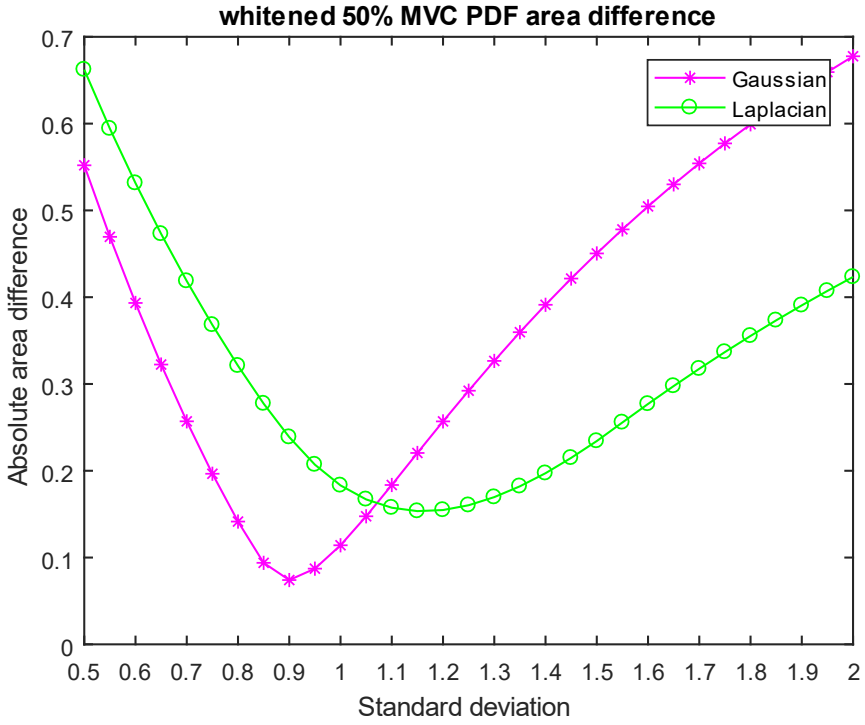

Figure 3.9 Absolute area difference versus standard deviation with both Gaussian and Laplacian (50% MVC unwhitened signal).

Based on the minimum absolute area difference of 0% MVC and 50% MVC, we provided the best fit of PDF estimate of 0% MVC and 50% MVC in Figure 3.10.

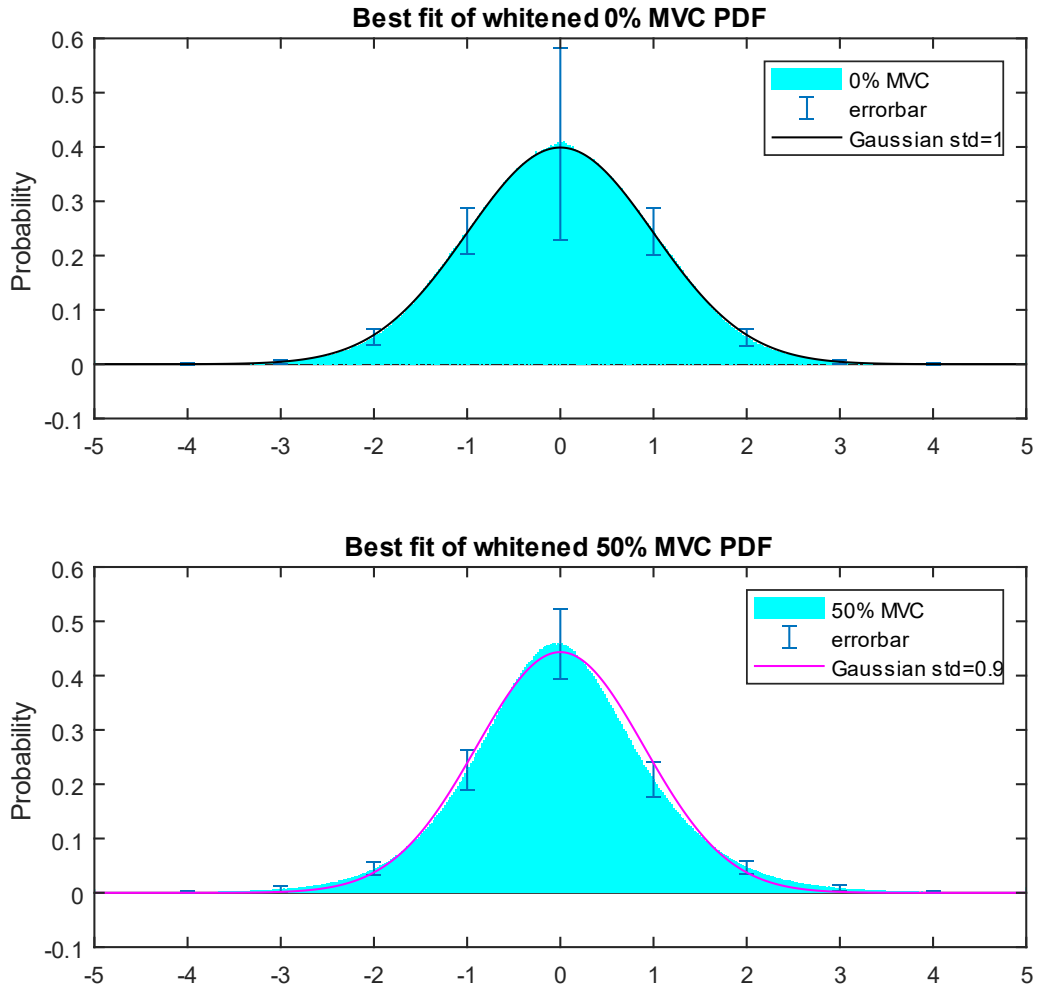

Figure 3.10 Best fit of whitened 0% MVC and 50% MVC PDF.

Based on the Table 3.1 and Table 3.2, we can notice that the rest contraction EMG signal is extremely well modeled as Gaussian, especially after whitening, which provides us confidence in this model of the rest contraction signal. For 50% MVC, the minimum absolute area difference comparing with Gaussian model is 0.0748 and 0.1535 with Laplacian model, neither Gaussian nor Laplacian model is as good as 0% MVC Gaussian model. For future work, it's reasonable to explore a combination of Gaussian and Laplacian model for higher contraction level EMG signals.

3.2 Power spectrum density of 0% MVC and 50% MVC EMG signal

Next, the 0% MVC and 50% MVC power spectrum density (PSD) estimations were produced by 512 subjects for each. Initially, we evaluated unwhitened signals. Each recording was sent through a fourth-order Butterworth highpass filter at 15-Hz cut-off frequency to remove the mean and attenuate motion artifacts. Then the first 500 ms was omitted to account for filter start-up transients. For normalization, we cannot use the same method as creating PDF estimation, because if we normalize both 0% MVC and 50% MVC to zero-mean and unit-variance random processes, we'll lose the power difference between the different force level.

So, two trials from the same subject and same electrode (0% MVC and 50% MVC) were divided by the standard deviation of the 50% MVC to preserve the relative power differences between 50% MVC and 0% MVC trials within the same subject and electrode. We used the Welch method (Hamming window, 50% overlap and 2048-length DFT) to form a PSD estimate for each recording. The ensemble sample mean PSD estimates of 0% MVC and 50% MVC recordings are shown in the same figure (Figure. 3.11).

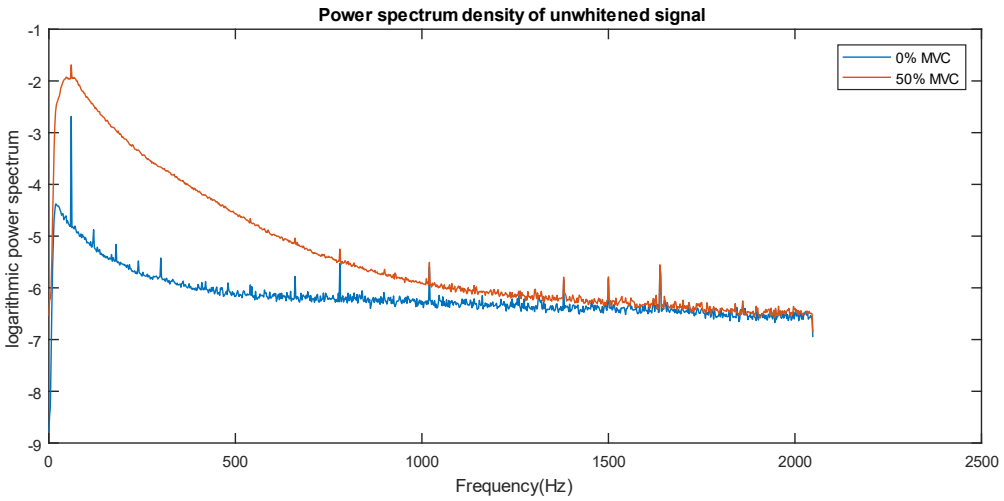

Figure 3.11 Power spectrum density of unwhitened 0% MVC and 50% MVC.

From the figure above we can notice that there are several spikes in the PSD which are caused by power-line interference. We used second-order IIR-notch filters to attenuate the power-line interference at some certain frequency locations corresponding to different subjects. The notch filter frequency locations and bandwidth are listed in Table 3.3 – Table 3.6 (PSD after notch filtering is in Figure 3.12).

Notch filter locations for different subjects:

Subject 'LA'

Frequency(Hz)	60	533.7	866.6	1031.1	1031.5	1446.8	1453.8	1638.9	1927.2
Bandwidth(Hz)	0.25	0.8	0.8	1.2	1.2	1.2	1.2	1.5	1.5

Table 3.3 Power-line attenuation frequency location and bandwidth of subject ‘LA’

Subject ‘LB’

Frequency(*59.97Hz)	1	2	3	5	6	7	8	9	11	13	15	16
Bandwidth(Hz)	0.25	0.25	0.25	0.25	0.25	0.25	0.25	0.8	0.8	0.8	0.8	0.8
Frequency(*59.97Hz)	17	19	20	21	23	24	25	27	29	30	31	33
Bandwidth(Hz)	1.2	1.2	1.2	1.2	1.2	1.2	1.2	1.5	1.5	1.5	1.5	1.5

Table 3.4 Power-line attenuation frequency location and bandwidth of subject ‘LB’

Subject ‘wx’

Frequency(*59.99Hz)	1	7	11	13	15	17	19	21
Bandwidth(Hz)	0.25	0.25	0.8	0.8	0.8	1.2	1.2	1.2
Frequency(*59.99Hz)	23	25	27	29	31	33	1996.5/59.99	
Bandwidth(Hz)	1.2	1.2	1.5	1.5	1.5	1.5	1.5	

Table 3.5 Power-line attenuation frequency location and bandwidth of subject ‘wx’

Subject ‘ww’

Frequency(*59.99Hz)	1	7	11	13	15	17	19	21
Bandwidth(Hz)	0.25	0.25	0.8	0.8	0.8	1.2	1.2	1.2
Frequency(*59.99Hz)	23	25	27	29	31	33	1996.5/59.99	
Bandwidth(Hz)	1.2	1.2	1.5	1.5	1.5	1.5	1.5	

Table 3.6 Power-line attenuation frequency location and bandwidth of subject ‘ww’

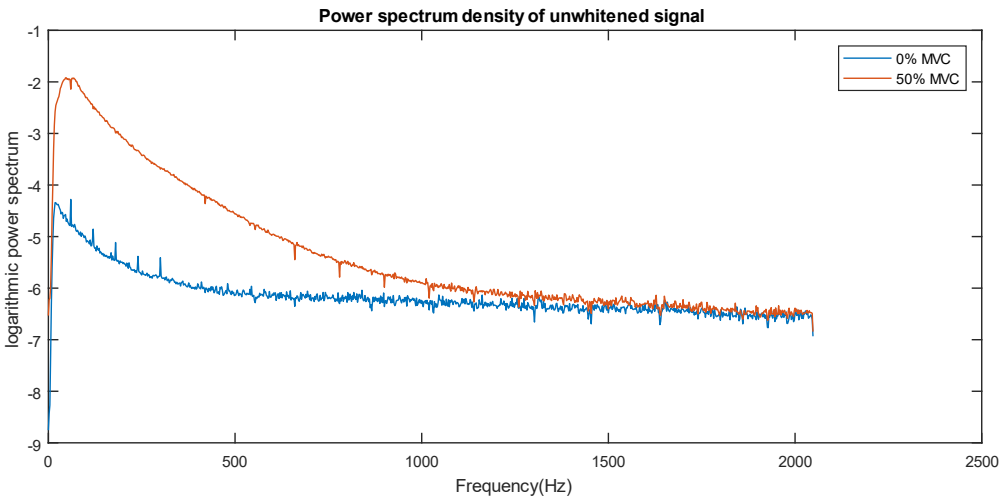

Figure 3.12 Power spectrum density of 0% MVC and 50% MVC after power-line attenuation.

Then, we estimate the power spectrum of whitened 0%MVC and 50% MVC signal. As above, each recording was sent through a fourth-order Butterworth highpass filter at 15-Hz cut-off frequency to remove the mean and attenuate motion artifacts, and then passed an adaptive whitening filter with band limit at 600 Hz, and IIR notch filtered to attenuate the power-line interference at the specific frequency locations described above. Then the first 500 ms were omitted to account for filter start-up transients. The whitening filter preserved the power differences between 0% MVC and 50% MVC. We used the Welch method (Hamming window, 50% overlap and 2048-length DFT) to form a PSD estimation for each recording. The ensemble sample mean PSD estimates of whitened 0% MVC and 50% MVC recordings are shown in the same figure (Figure 3.13 shows the PSD of whitened signal).

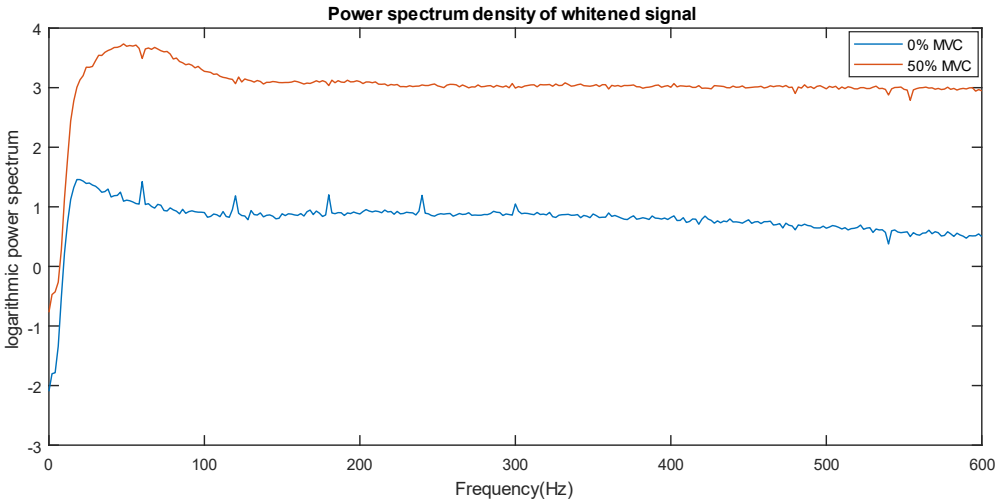

Figure 3.13 Power spectrum density of whitened 0% MVC and 50% MVC.

4. Probability of estimating a zero-value in Gaussian model rest contraction

(The mathematical analysis was first derived by Prof.Clancy. The description follows his calculation process and replicates the math.)

Chapter 3 shows that the empirical PDF of rest (0% MVC) EMG is very close to Gaussian. So, in this chapter we use a Gaussian model to estimate EMGσ during rest.

In general, the measured EMG signal during constant-force contraction follows the amplitude modulated model:

$$m[n] = s \cdot x[n] + v[n], \quad 0 \le n < N \tag{1}$$

where n is the discrete-time sample index, s is the standard deviation of true EMG, $(s \cdot x[n])$ is the noise-free EMG signal and $v[n]$ is additive noise (i.e., the signal recorded when the muscle is at rest). Let $x[n]$ and $v[n]$ be jointly Gaussian random vectors that are both uncorrelated, zero-mean, wide-sense stationary and correlation-ergodic; the only difference is $x[n]$ has unit variance but $v[n]$ is of variance equal to q^2. $m[n]$ is a jointly Gaussian random vector with zero mean and a covariance matrix equal to: $K_{\underline{mm}} = \sigma_m^2 \, I$, where $\sigma_m^2 = s^2 + q^2$ and I is the identity matrix. Then use the maximum likelihood estimate method to determine the optimal estimate of s $(\mathrm{i.e.,EMG}\sigma)$.

The probability density function (PDF) for zero-mean vector $m[n]$, given that the standard deviation of the true EMG is the known value $\hat{s}$ is:

$$p_{\underline{m}|s}(\underline{M}|\hat{s}) = \frac{e^{\frac{-\underline{M}^T K_{\underline{mm}}^{-1} \underline{M}}{2}}}{(2\pi)^{N/2} \left|K_{\underline{mm}}\right|^{1/2}} = \frac{e^{\frac{-\sum_{n=0}^{N-1} M[n]^2}{2(\hat{s}^2+q^2)}}}{[2\pi(\hat{s}^2+q^2)]^{N/2}}, \tag{2}$$

where $\underline{M}$ denotes an instance of the random vector and $-\infty \le M_n \le \infty$.

The maximum likelihood estimate of the standard deviation is the value of $\hat{s}$ which maximizes the above density. Takes the natural logarithm of (2):

$$\ln\left[p_{\underline{m}|s}(\underline{M}|\hat{s})\right] = -\frac{N}{2}\ln(2\pi) - \frac{N}{2}\ln(\hat{s}^2 + q^2) - \frac{\sum_{n=0}^{N-1} M[n]^2}{2(\hat{s}^2+q^2)}. \tag{3}$$

Differentiating equation(3) with respect to $\hat{s}$ gives:

$$\frac{\partial \ln\left[p_{\underline{m}|s}(\underline{M}|\hat{s})\right]}{\partial \hat{s}} = -\frac{N}{2}\frac{2\hat{s}}{\hat{s}^2+q^2} + \frac{\hat{s}\sum_{n=0}^{N-1} M[n]^2}{(\hat{s}^2+q^2)^2}. \tag{4}$$

Setting the derivative to zero and solving for $\hat{s}$:

$$\hat{s} = \sqrt{\left(\frac{\sum_{n=0}^{N-1} M[n]^2}{N}\right) - q^2}. \tag{5}$$

This equation means we subtract noise in the power domain. The term inside the round parentheses is the mean square value of the EMG signal.

Evaluation of the second derivative of (3), with respect to $\hat{s}$, verifies that (5) is indeed a local maximum —but only when the RMS in (5) exceeds the noise variance q^2. This condition is almost always satisfied during active muscle contraction, but not during low-level contractions or rest. For such a case, maximization with respect to $\hat{s}$ of the PDF occurs at the boundary constraint where $\hat{s} = 0$. Hence, the complete solution for this estimator is:

$$\hat{s}_{\mathrm{RMS}} = \sqrt{\max\left[0,\ \left(\frac{\sum_{n=0}^{N-1} M[n]^2}{N}\right) - g^2 q^2\right]}, \tag{6}$$

where *g≥0* is a gain factor that scales the subtraction term. The maximum likelihood estimate is found when g = 1.

Denote the term in the rounded parenthesis of (6) as random variable *y*. Note that when the muscle is at rest, $s = 0$ and *y* is Gamma distributed as:

$$p_{y,Rest}(Y) = \begin{cases} \dfrac{Y^{\frac{N}{2}-1}\, e^{\frac{-Y\cdot N}{2q^2}}}{\left(q\sqrt{\frac{2}{N}}\right)^N \Gamma\left(\frac{N}{2}\right)}, & Y > 0 \\ 0, & \text{otherwise} \end{cases}. \tag{7}$$

Further, the probability of estimating a zero value during rest is the cumulative density function (CDF) of *y*, evaluated at $Y = g^2 q^2$. This CDF, for *N* even, is:

$$P_{y \le g^2 q^2, Rest}(Y)\big|_{Y=g^2 q^2, s=0} = 1 - \sum_{k=0}^{\frac{N}{2}-1} \frac{\left(\frac{N}{2}\right)^k\ g^{2k}\ e^{\frac{-g^2 N}{2}}}{k!}, \quad Y > 0, N \text{ even}. \tag{8}$$

Note that this probability is only a function of *N*. This result shows that the probability of estimating a zero value is unrelated to the standard deviation of the noise—it is only related to the smoothing window length. The probability of estimating a zero value versus smoothing window length is shown in Figure 4.1.

Based on the theoretical result from equation (8), we computed the probability of estimating zero values with window length ranges from 10 to 200. When the window length equals to 200, when g=1, 51.33% of the EMGσ estimates are zero, 84.73% of estimates are zero when g=1.05, and only 16.48% are zero when g=0.95.

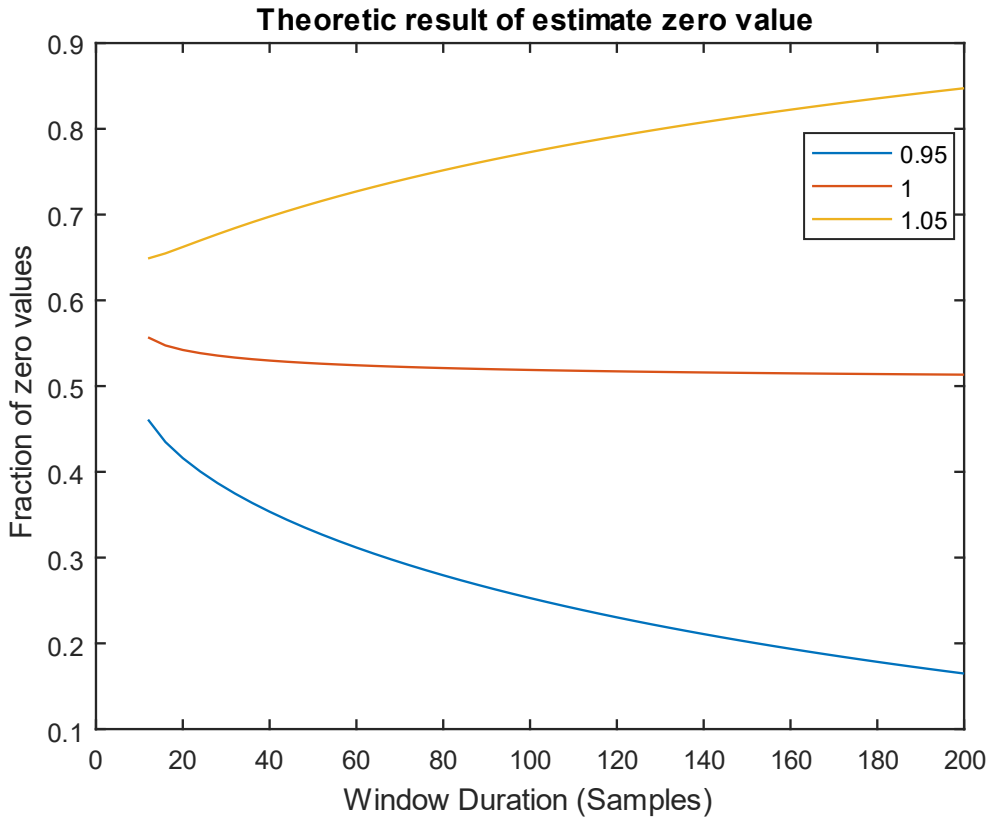

Figure 4.1 Theoretic result of fraction of zero values versus window duration.

For g=1, we only have around 50% possibility to estimate EMGσ = 0 during rest. In rest contractions, we intuitively desire an EMGσ estimate of zero with higher probability. For example, myoelectric prosthesis control software very much desires a control signal that equals zero whenever the user's muscles are at rest. Else, the prosthesis will slowly "drift" and change its posture when the user intends the device to remain in its current pose. A reasonable approach to further increase the probability of a zero output during muscle rest is to increase the gain factor "g".

We empirically computed the fraction of times in which a zero EMGσ value was found during test with three different gain factors, which are g greater, equal and less than 1, respectively. Using the RMS processor described in equation (6), we computed the fraction of estimated zero values versus window length with g equal to 0.95, 1 and 1.05 separately. We used 512 whitened 0% MVC recordings. Each recording was highpass filtered by a fourth-order Butterworth filter at 15-Hz cut-off frequency to remove mean and attenuate motion artifacts and passed through an adaptive whitening filter [14] with bandwidth limited at 600 Hz. Then the first 500 ms was omitted to remove filter start-up transients. We then applied the RMS processer described as equation (6) to estimate EMGσ, evaluating the fraction of

samples were zero-valued for each subject, using each gain factor. The q^2 fraction in equation (6) was estimated for each recording as its sample variance. We varied the window length from 10 samples to 1250 samples (Sample frequency is 4096 Hz) The ensemble mean and standard deviation computed through 512 recordings are shown in Figure 4.2.

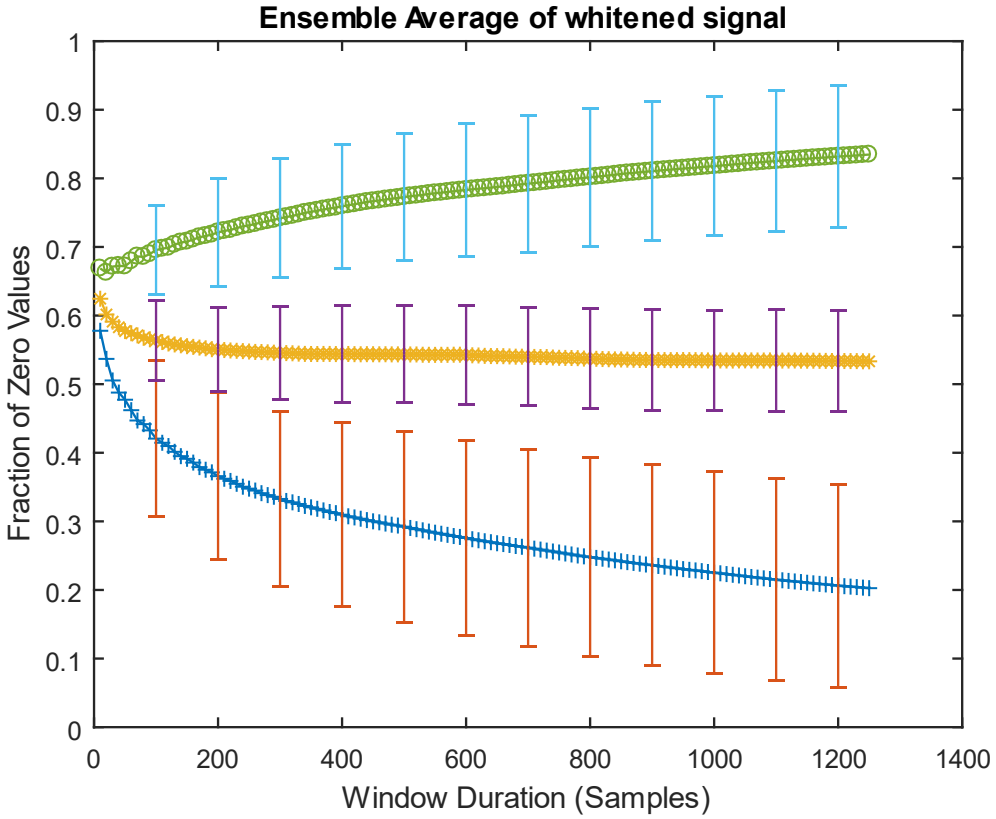

Figure 4.2 Fraction of zero values. (Yellow "-*" with purple error bar is "g = 1", green "-o" with blue error bar is "g = 1.05", blue "-+" with orange error bar is "g = 0.95")

As we can see from the plot, the result from 512 0% MVC subjects has the same trend comparing with theoretical result at each "g" value. The only difference is the length of x-axis. The theory assumed perfectly uncorrelated samples, the correlation of true data leads to a longer x-axis.

As we described in chapter 1, a longer window length is suitable for slow EMGσ changes, since this thesis used constant-force data, a larger window duration is appropriate. As window length increases to 1250, when g=1, 53.33% of the EMGσ estimates are zero, 83.47% of estimates are zero when g=1.05, and only 20.26% are zero when g=0.95. In conclusion, we could increase a gain factor applied to noise during the power domain subtraction to ensure we have a larger portion of zero EMGσ values during rest. Of course, we do so at the cost of suppressing low EMGσ values.

5. Conclusion and future prospects

By using adaptive whitening filter to improve EMG amplitude estimation, we successfully replaced the subject-specific whitening filter by a universal whitening filter without performance loss. This simplified whitening filter has the same quality as the original adaptive whitening filter, which overcome the low-contraction noise issue of conventional linear whitening filters. The omitted the calibration step for each subject eases implementation of the whitening filter. And there are still prospects to further improve universal whitening. For example, the general shape of the universal fixed whitening filter is high-pass filter, thus we could find a conventional FIR filter that has similar shape, so that instead of saving and loading the coefficient matrix, we can directly use a FIR filter design to achieve the same effect.

The rest contraction modeling showed that the resting EMG signal is extremely well modeled as Gaussian, with only a 1.6% difference compared to the ideal Gaussian distribution. The new RMS estimator (with gain “g” multiplied by the noise standard deviation) addresses the drifting problem of prosthesis control during rest. On the other hand, the 50% MVC model is less accurate. Neither the Gaussian distribution nor the Laplacian distribution had a PDF area difference between real 50% MVC probability distribution below 7%. Because the rest EMG is more Gaussian, and EMG with active force has a PDF that is more Laplacian, we could investigate the combination of Gaussian and Laplacian distribution to modulate 50% MVC in future work.

6. Conference paper (Author's copy)

Simplified Implementation of Optimized Whitening of the Electromyogram Signal

He Wang[1], Kiriaki J. Rajotte[1], Haopeng Wang[1], Chenyun Dai[2], Ziling Zhu[1], Moinuddin Bhuiyan[1], Edward A. Clancy[1]

[1] Worcester Polytechnic Institute (WPI), USA; [2]Fudan University, China

Introduction: The surface electromyogram (EMG) signal is well modeled as an amplitude modulated, correlated random process. The amplitude modulation, defined as the time-varying standard deviation (EMGσ) of the signal, is used in various applications as a measure of muscle effort, e.g., EMG-force models, prosthesis control, clinical biomechanics and ergonomics assessment. EMGσ can be estimated by rectifying the EMG and then lowpass filtering (cutoff ~1 Hz). However, it has long been known that the correlated nature of EMG reduces the statistical efficiency of the EMGσ estimate, producing a large variance.

To combat this problem, a whitening filter can be used prior to the rectifier. Whitening removes signal correlation—while preserving signal standard deviation—producing a substantially improved EMGσ. The ad-vantages of whitening filters have been known since at least 1974 [3]—yet, few researchers use them. A key limitation to widespread use is that most whiteners are "calibrated" to each subject, making them cumbersome to implement.

Since EMG whitening filters have low gain at low frequencies and higher gain at high frequencies, Potvin [4] implemented simple whitening via a fixed, low-order, FIR, highpass filter that was not calibrated to individual sub-jects. This approach was not compared to the established technique of subject-specific whitening filters.

Our work reported herein describes development of a simplified whitening technique that relies only on EMG magnitude normalization (a measure that is already common). We compare this technique to state-of the art subject-specific whitening.

Experimental Methods: Pre-existing data from 64 sub-jects [5] were used and did not require human studies supervision per the WPI IRB. Four electrodes over the biceps and four over the triceps muscles were acquired during three trials of 30-s duration, constant-posture, force-varying elbow contractions in which subjects followed a target displaying a 1 Hz bandlimited, uniform and random process, spanning 50% maximum voluntary contraction (MVC) flexion to 50% MVC extension. Using our existing subject-specific technique to form whitening filters for each electrode (calibrated from additional 5-s rest recordings and constant-effort 50% MVC trials, and limited to 600 Hz in frequency [6,7]), we related EMGσ to force. This EMGσ-force

model used each of the eight EMGσ values as inputs, a 15th-order dynamic FIR model per EMGσ, additionally included the squared value of each EMGσ at the 15 time lags (to model the EMG-force non-linearity), and was trained from two trials using least squares. The average ± std. dev. test error on the distinct third trials was 4.84±1.98% flexion MVC (%MVCF). This error served as our "baseline" performance.

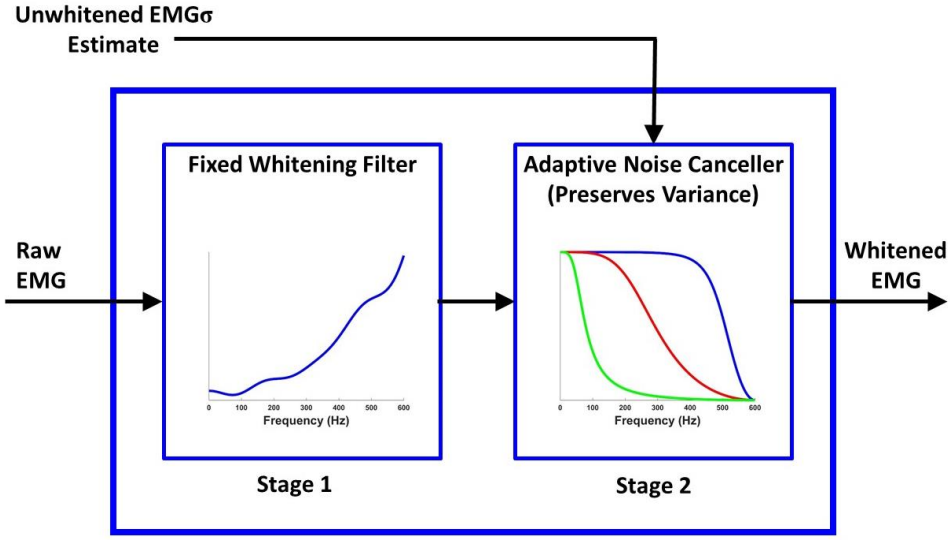

Fig. 1. Two-stage adaptive whitening filter [6].

Analysis Methods and Results: Our whitening filters (Fig. 1) are comprised of a fixed whitening filter followed by an adaptive noise canceller (with variance preservation). The first stage is a fixed linear filter whose magnitude response is the inverse of the square root of the power spectral den-sity (PSD) of the noise-free EMG signal (estimated by subtracting the 0% MVC PSD from the 50% MVC PSD). This filter has low gain at low frequencies and higher gain at high frequencies—the opposite of the spectral content of EMG. The second stage cancels high frequency noise, above the dominant frequency of EMG. This filter is a time-varying lowpass filter, with a cut-off frequency that is lower at lower effort levels. This filter also provides a gain that preserves the overall power of the noise-free signal, so that the full whitening process does not alter EMGσ.

We contrasted subject-specific whitening filter calibration to "universal" calibration. Each EMG was gain normalized, to account for gain variations between channels. Thereafter, the 0% MVC PSDs and (separately) the 50% MVC PSDs were ensemble-averaged across the 512 calibration recordings (64 subjects x 8 electrodes/subject). The one, ensemble-averaged 0% MVC and the one, ensemble-averaged 50% MVC were then used to form a single "universal" two-stage whitening filter. This filter was then similarly evaluated on the EMG-force data,

producing an average ± std. dev. test error of 4.80±2.03 %MVCF—essentially identical to the performance found when using the subject-specific whitening filters.

Conclusions: Our work, combined that of Potvin [4], suggests that the PSD of EMG is sufficiently consistent subject-to-subject that subject-specific calibration of PSDs for EMG whitening may not be necessary (for noise cancellation). Only a gain normalization may be needed per channel. Note that PSD shapes are known to vary with inter-electrode distance [1] and might vary muscle-to-muscle. Also, this set of dynamic contractions may not be particularly sensitive to the magnitude of the noise power, since few of the active-trial contractions were near 0% MVC. (Noise is most impactful at low contraction levels.)

References:

1. Hogan N et al. IEEE TBME. 1980;27:396–410.
2. Clancy EA et al. IEEE TBME. 1995;42:203–211.
3. Kaiser E et al. In “Control of Upper-Extremity Prosthetics & Ortho.,” Charles C. Thomas, 1974:54–57.
4. Potvin et al. J Electromyo Kinesiol. 2004;14:389–399.
5. Dai et al. IEEE TNSRE. 2017;25:1529–1538.
6. Clancy et al. IEEE TBME. 2000;47:709–719.
7. Dasog et al. IEEE TNSRE. 2014;22:664-670.

References

[1] https://en.wikipedia.org/wiki/Electromyography

[2] https://en.wikipedia.org/wiki/Muscle_fascicle

[3] http://academic.wsc.edu/faculty/jatodd1/351/ch6outline.html

[4] http://www.physicsforums.com/showthread.php?t=473984

[5] DeLuca, "Physiology and mathematics of myoelectric signals," IEEE Trans Biomed Eng 26(6): 313–325, 1979.

[6] M. B. I. Raez, M. S. Hussain, and F. Mohd-Yasin, “Techniques of EMG signal analysis: Detection, processing, classification and applications,” Biol. Proced. Online, vol. 8, pp. 11–35, 2006.

[7] D. Staudenmann, K. Roeleveld, D. F. Stegeman, and J. van Dieen, “Methodological aspects of SEMG recordings for force estimation—A tutorial and review,” J. Electromyogr. Kinesiol., vol. 20, pp. 375–387,2010.

[8] Edward A. Clancy and Neville Hogan, "Relating Agonist-Antagonist Electromyograms to Joint Torque During Isometric, Quasi-Isotonic, Non-Fatiguing Contractions," IEEE Transactions on Biomedical Engineering, Vol. 44, No. 10, pp. 1024-1028, 1997.

[9] Edward A. Clancy, Stochastic Modeling of the Relationship Between the Surface Electromyogram and Muscle Torque. Ph.D. Thesis, Massachusetts Institute of Technology, January 1991.

[10] E. A. Clancy, ECE5341 “Applied Medical Signal Processing” Lecture “Relating Surface EMG to Joint Torque”, Worcester Polytechnic Institute, 2015.

[11] Edward A. Clancy, Evelyn L. Morin and Roberto Merletti, "Sampling, Noise-Reduction and Amplitude Estimation Issues in Surface Electromyography," Journal of Electromyography and Kinesiology, Vol. 12, No. 1, pp. 1–16, 2002.

[12] Hogan, N. and R. W. Mann, "Myoelectric signal processing: Optimal estimation applied to electromyography-Part II: Experimental demonstration of optimal myoprocessor performance," IEEE Trans. Biomed. Eng., vol. BME-27, pp. 396-410, 1980b.

[13] Harba, M. I. A. and P. A. Lynn, "Optimizing the acquisition and processing of surface electromyographic signals," J. Biomed. Eng., vol. 3, pp. 100-106, 1981.

[14] Edward A. Clancy and Kristin A. Farry, "Adaptive Whitening of the Electromyogram to Improve Amplitude Estimation," IEEE Transactions on Biomedical Engineering, Vol. 47, No. 6, pp. 709-719, 2000.

[15] Hogan, N. and R. W. Mann, "Myoelectric signal processing: Optimal estimation applied to electromyography-Part I: Derivation of the optimal myoprocessor," IEEE Trans. Biomed. Eng., vol. BME-27, pp. 382-395, 1980a.

[16] Edward A. Clancy and Neville Hogan, "Multiple Site Electromyograph Amplitude Estimation," IEEE Transactions on Biomedical Engineering, Vol. 42, No. 2, pp. 203-211, 1995.

[17] Edward A. Clancy, Stéphane Bouchard and Denis Rancourt, "Estimation and Application of Electromyogram (EMG) Amplitude During Dynamic Contractions," IEEE Engineering in Medicine and Biology Magazine, Vol. 20, No. 6, pp. 47-54, 2001.

[18] Edward A. Clancy and Neville Hogan, "Relating Agonist-Antagonist Electromyograms to Joint Torque During Isometric, Quasi-Isotonic, Non-Fatiguing Contractions," IEEE Transactions on Biomedical Engineering, Vol. 44, No. 10, pp. 1024-1028, 1997.

[19] Pu Liu, Lukai Liu, Francois Martel, Denis Rancourt and Edward A. Clancy, "Influence of Joint Angle on EMG-Torque Model During Constant-Posture Quasi-Constant-Torque Contractions," Journal of Electromyography and Kinesiology, Vol. 23, No. 5, pp. 1020–1028, 2013.

[20] Edward A. Clancy, "Electromyogram Amplitude Estimation with Adaptive Smoothing Window Length," IEEE Transactions on Biomedical Engineering, Vol. 46, No. 6, pp. 717-729, 1999.

[21] Chenyun Dai, Berj Bardizbanian and Edward A. Clancy, "Comparison of Constant-Posture Force-Varying EMG-Force Dynamic Models About the Elbow," IEEE Transactions on Neural Systems and Rehabilitation Engineering, Vol. 25, No. 9, pp. 1529–1538, 2017.

[22] K. Nazarpour, A. H. Al-Timemy, G. Bugmann, and A. Jackson, “A note on the probability distribution function of the surface electromyogram signal,” Brain Res. Bull., vol. 90, pp. 88–91, 2013.

[23] Rodriguez-Falces J. Understanding the electrical behavior of the action potential in terms of elementary electrical sources. Adv Physiol Educ 39: 15–26, 2015. doi:10.1152/advan.00130.2014

[24] Muthukumaraswamy, S.D. High-frequency brain activity and muscle artifacts in MEG/EEG: a review and recommendations. Front. Hum. Neurosci. 7, 138(2013).

[25] R. H. Chowdhury, M. B. Reaz, M. A. B. M. Ali, A. A. Bakar, K. Chellappan, and T. G. Chang, “Surface electromyography signal processing and classification techniques,” Sensors, vol. 13, no. 9, pp. 12431–12466, 2013.

[26] RobertsTJ, GabaldonAM.Interpreting muscle function from EMG: lessons learned from direct measurements of muscle force. Integ Comp Biol 2008; 48: 312-20.

[27] https://en.wikipedia.org/wiki/Action_potential

[28] https://www.sciencedirect.com/topics/medicine-and-dentistry/myoelectricity

[29] Edward A. Clancy, Stéphane Bouchard and Denis Rancourt, "Estimation and Application of Electromyogram (EMG) Amplitude During Dynamic Contractions," IEEE Engineering in Medicine and Biology Magazine, Vol. 20, No. 6, pp. 47-54, 2001.

[30] Potvin, J.R., and Brown, S. 2004. Less is more: high-pass filtering, to remove up to 99% of the surface EMG signal power, improves EMG-based biceps brachii muscle force estimates. J. Electromyogr. Kinesiol. 14: 389–399. doi:10.1016/j.jelekin. 2003.10.005. PMID:15094152.

Appendix

Appendix I Subjects used in this thesis

Experiment ‘LA’

'01'; '02'; '03'; '04'; '05'; '06'; '07'; '10'; '13'; '14'; '15'; '16'; '17'; '18'; '19'; '20'; '21';

Trial number for 0%MVC and 50% MVC extension and flexion

Trial ‘15’ 0%MVC

Trial ’10’ 50% Extension

Trial ‘12’ 50% Flexion

We found subject ‘LA18’ trial ‘15’ is a bad rest recording, we substitute this recording by trial ‘32’ of subject ‘LA18’

Experiment ‘LB’

'02'; '03'; '05'; '07'; '08'; '09'; '10'; '12'; '13'; '16'; '17'; '18'; '19'; '20'; '21';

Trial number for 0%MVC and 50% MVC extension and flexion

Trial ‘15’ 0%MVC

Trial ’10’ 50% Extension

Trial ‘12’ 50% Flexion

Experiment ‘wx’

'01'; '02'; '04'; '05'; '06'; '07'; '08'; '09'; '10'; '11'; '12'; '13'; '14'; '17'; '18'; '19'; '20'; '22'; '23'; '24'; '25'

Trial number for 0%MVC and 50% MVC extension and flexion

Trial ‘15’ 0%MVC

Trial ’10’ 50% Extension

Trial ‘13’ 50% Flexion

Experiment ‘ww’

'01'; '02'; '03'; '04'; '05'; '06'; '08'; '09'; '10'; '11'; '12']

Trial number for 0%MVC and 50% MVC extension and flexion

Trial ‘15’ 0%MVC

Trial ’10’ 50% Extension

Trial ‘12’ 50% Flexion

We found subject ‘ww05’ trial ‘15’ is a bad rest recording, we substitute this recording by trial ‘39’ of subject ‘ww05’

Appendix II EMG-torque model testing

EMG-torque model testing mentioned in chapter 2 was based on Dr. Dai's work and publication. He tested different techniques and parameters of the EMG-torque model, we used one of his model, which is 1x8 channel, 15th-order quadratic model with the tolerance of 0.0056. The abstract and introduction of his publication are listed below with important graphic result:

Chenyun Dai, Berj Bardizbanian and Edward A. Clancy, "Comparison of Constant-Posture Force-Varying EMG-Force Dynamic Models About the Elbow," IEEE Transactions on Neural Systems and Rehabilitation Engineering, Vol. 25, No. 9, pp. 1529–1538, 2017.

Abstract—Numerous techniques have been used to minimize error in relating the surface electromyogram (EMG) to elbow joint torque. We compare the use of three techniques to further reduce error. First, most EMG-torque models only use estimates of EMG standard deviation as inputs. We studied the additional features of average waveform length, slope sign change rate and zero crossing rate. Second, multiple channels of EMG from the biceps, and separately from the triceps, have been combined to produce two low-variance model inputs. We contrasted this channel combination with using each EMG separately. Third, we previously modeled nonlinearity in the EMG-torque relationship via a polynomial. We contrasted our model vs. that of the classic exponential power law of Vredenbregt and Rau. Results from 65 subjects performing constant-posture, force-varying contraction gave a "baseline" comparison error (i.e., error with none of the new techniques) of 5.5 ± 2.3% maximum flexion voluntary contraction (%MVCF). Combining the techniques of multiple features with individual channels reduced error to 4.8 ± 2.2 %MVCF, while combining individual channels with the power-law model reduced error to 4.7 ± 2.0 %MVCF. The new techniques further reduced error from that of the baseline by ≈15%.

Example EMGσ-torque estimation results for selected models. Butterworth model (2 Hz lowpass filter cut-off) exhibited an RMS error of 10.2 %MVC. Eight-channel EMGσ model (Q = 15 order, pseudo-inverse tolerance of Tol = 0.005) exhibited an RMS error of 4.5 %MVC. "Truth" refers to the recorded load cell values. Subject LA04, trial 45. Shown in figure below.

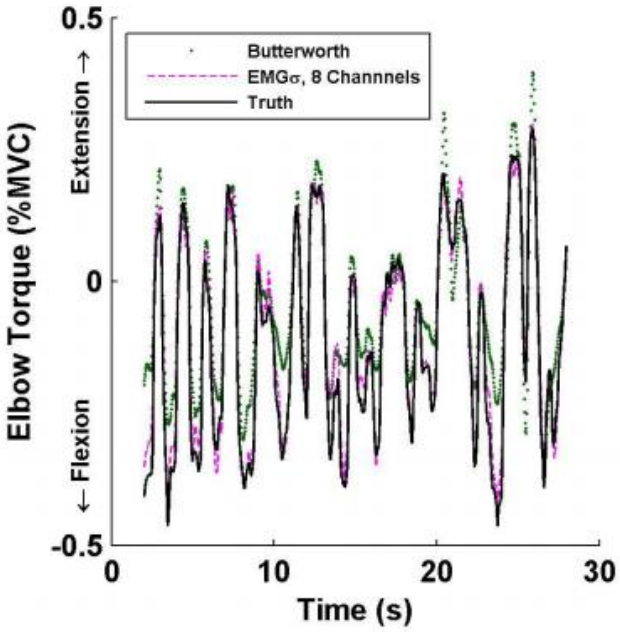

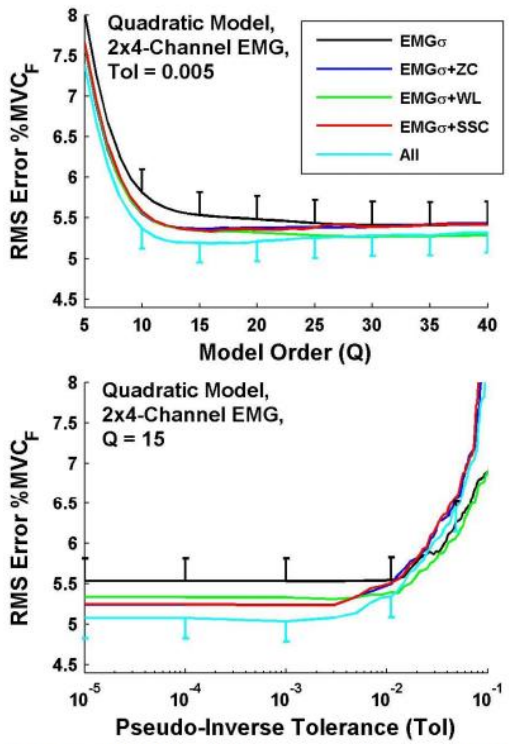

Fig. 3. Baseline Model vs. Feature Set: Average RMS errors from 65 subjects, four-channel EMG. Legend refers to both plots. Single-sided standard error bars shown for two of five feature sets (standard errors were similar for the other three feature sets) for selected Q values. Top: Results vs. quadratic model order (Q), using pseudo-inverse tolerance of Tol=0.005. Bottom: Results vs. pseudo-inverse tolerance, with quadratic model order Q=15.

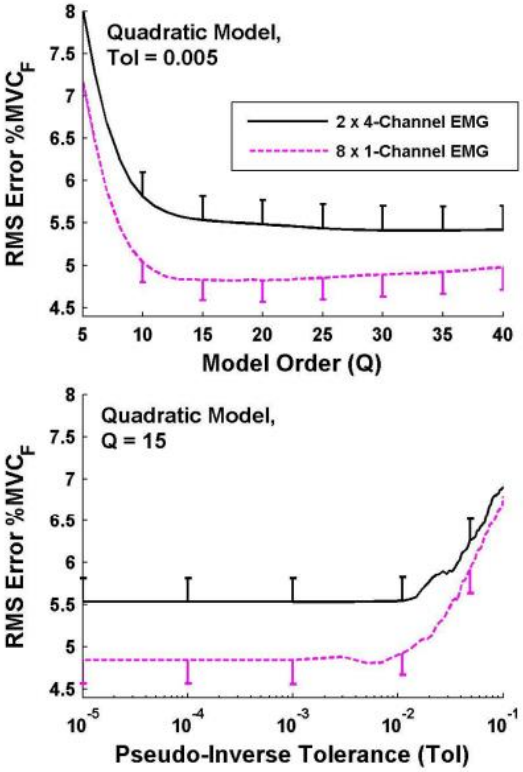

Fig. 4. Baseline Model vs. EMG Channel Selection: Average RMS errors from 65 subjects, EMGσ-only feature set. Single-sided standard error bars shown for selected Q values. Top: Results vs. quadratic model order (Q), using pseudo-inverse tolerance of Tol= 0.005. Bottom: Results vs. pseudo-inverse tolerance, with quadratic model order Q=15.

Appendix III Gaussian Model, Rest contractions (Written by Edward A. Clancy, Included with Permission)

(Derivation of the optimal processor from this case is from (Clancy, 1991)). Consider an amplitude modulated model of the measured EMG signal, m[n], during constant-effort contraction as:

$$m[n] = s \cdot x[n] + v[n], \quad 0 \le n < N$$

where n is the discrete-time sample index, s is the standard deviation (i.e., modulation) of the noise-free (true) EMG, $(s \cdot x[n])$ is the noise-free EMG signal and $v[n]$ is additive noise (i.e., the signal recorded when the muscle is at rest). Let $x[n]$ be zero mean, unit-variance, wide-sense stationary and correlation-ergodic. Let $v[n]$ be a similarly specified, but of variance equal to q^2. Variables $x[n]$ and $v[n]$ are assumed to have uncorrelated samples (via pre-whitening) and be independent. Let $\underline{m}$, $\underline{x}$ and $\underline{v}$ be vectors comprised of N samples of each respective random variable.

Let both $\underline{x}$ and $\underline{v}$ be jointly Gaussian random vectors. With these assumptions, $\underline{m}$ is a jointly Gaussian random vector with zero mean and a covariance matrix equal to: $K_{\underline{mm}} = \sigma_m^2 \, I$, where $\sigma_m^2 = s^2 + q^2$ and I is the identity matrix. Thus, the probability density function (PDF) for zero-mean vector $\underline{m}$, given that the standard deviation of the true EMG is the known value $\hat{s}$ is:

$$p_{\underline{m}|s}\left(\underline{M}|\hat{s}\right) = \frac{e^{\frac{-\underline{M}^T K_{\underline{mm}}^{-1} \underline{M}}{2}}}{(2\pi)^{N/2} \left|K_{\underline{mm}}\right|^{1/2}} = \frac{e^{\frac{-\sum_{n=0}^{N-1} M[n]^2}{2(\hat{s}^2+q^2)}}}{[2\pi(\hat{s}^2+q^2)]^{N/2}},$$

where $\underline{M}$ denotes an instance of the random vector and $-\infty \le M_n \le \infty$.

The maximum likelihood estimate of the standard deviation is the value of $\hat{s}$ which maximizes the above density. A monotonic transformation of the PDF does not alter the location of the maximum. Thus, taking the natural logarithm yields:

$$\ln\left[p_{\underline{m}|s}\left(\underline{M}|\hat{s}\right)\right] = -\frac{N}{2} \ln(2\pi) - \frac{N}{2} \ln(\hat{s}^2 + q^2) - \frac{\sum_{n=0}^{N-1} M[n]^2}{2(\hat{s}^2+q^2)}.$$

Differentiating the above with respect to $\hat{s}$ gives:

$$\frac{\partial \ln\left[p_{\underline{m}|s}\left(\underline{M}|\hat{s}\right)\right]}{\partial \hat{s}} = -\frac{N}{2} \frac{2\hat{s}}{\hat{s}^2+q^2} + \frac{\hat{s} \sum_{n=0}^{N-1} M[n]^2}{(\hat{s}^2+q^2)^2}.$$

Setting this derivative to zero and manipulating leads to a quadratic equation for $\hat{s}^2$, the square root of which provides our result. The quadratic equation has two solutions. But, one of these solutions is not real-valued, so can be eliminated. The retained result is:

$$\hat{s} = \sqrt{\left(\frac{\sum_{n=0}^{N-1} M[n]^2}{N}\right) - q^2}.$$

The left-hand term within the square root is the RMS value. Hence, the noise "offset" correction is made in the power domain.

Evaluation of the second derivative of (3), with respect to $\hat{s}$, verifies that (5) is indeed a local maximum (and *not* a minimum)—but only when the RMS in (5) exceeds the noise variance q^2. This condition is almost always satisfied during active muscle contraction, but not during low-level contractions or rest. For such a case, maximization with respect to $\hat{s}$ of the PDF occurs at the boundary constraint where $\hat{s} = 0$. Hence, the complete solution for this estimator is:

$$\hat{s}_{\mathrm{RMS}} = \sqrt{\max\left[0,\ \left(\frac{\sum_{n=0}^{N-1} M[n]^2}{N}\right) - q^2\right]}, \tag{6}$$

where "max" denotes the maximum value operator and the "RMS" subscript emphasizes the use of an RMS processor.

The term inside the rounded parentheses can be re-written as:

$$y = \sum_{n=0}^{N-1} \left(\frac{M[n]}{\sqrt{N}}\right)^2,$$

where the new random variables $\frac{M[n]}{\sqrt{N}}$ are jointly Gaussian, white (thus, for Gaussian random variables, independent), wide-sense stationary, correlation-ergodic, zero-mean and of standard deviation $\frac{\sigma_m}{\sqrt{N}}$. In general, Papoulis (Papoulis, 1984) showed that if $\underline{x}$ is an *N*-length, jointly Gaussian, white, wide-sense stationary, correlation-ergodic, random vector of zero mean and standard deviation σ, then $y = \sum_{n=0}^{N-1} x^2[n]$ is Chi-square distributed as:

$$p_y(Y) = \begin{cases} \dfrac{Y^{\frac{N}{2}-1}\, e^{\frac{-Y}{2\sigma^2}}}{\left(\sigma\sqrt{2}\right)^N \Gamma\left(\frac{N}{2}\right)}, & Y > 0 \\ 0, & \text{otherwise,} \end{cases}$$

where $\Gamma(\cdot)$ is the Gamma function, defined for α positive as:

$$\Gamma(\alpha) = \int_{x=0}^{\infty} x^{\alpha-1}\, e^{-x}\, dx, \quad \alpha > 0.$$

Note that if α is a positive integer, $\Gamma(\alpha) = (\alpha - 1)!$. Substituting the known value for the standard deviation of the original Gaussian variables gives:

$$p_y(Y) = \begin{cases} \dfrac{Y^{\frac{N}{2}-1}\, e^{\frac{-Y \cdot N}{2\sigma_m^2}}}{\left(\sigma_m \sqrt{\dfrac{2}{N}}\right)^N \Gamma\left(\dfrac{N}{2}\right)}, & Y > 0 \\ 0, & \text{otherwise.} \end{cases}$$

Miller and Freund (Miller & Freund, 1977) list this distribution as the Gamma PDF [as does Papoulis (Papoulis, 1984), albeit with distinct notation], as:

$$p_x(X) = \begin{cases} \dfrac{X^{a-1}\, e^{\frac{-X}{b}}}{b^a\, \Gamma(a)}, & X > 0,\ a > 0,\ b > 0 \equiv \text{Gamma}(a, b), \\ 0, & \text{otherwise} \end{cases}$$

where $E(x) = ab$ and $\sigma_x^2 = a\, b^2$. Comparison of the numerators of $p_x(X)$ and $p_y(Y)$ shows that $a = \frac{N}{2}$ and $b = \frac{2\,\sigma_m^2}{N}$. As a check, substituting these values into the denominator of $p_x(X)$ correctly equates to the denominator of $p_y(Y)$:

$$b^a\, \Gamma(a) = \left(\frac{2\,\sigma_m^2}{N}\right)^{\frac{N}{2}} \Gamma\left(\frac{N}{2}\right) = \left(\sigma_m \sqrt{\frac{2}{N}}\right)^N \Gamma\left(\frac{N}{2}\right), \quad \sigma_m \geq 0.$$

Hence, the moment formulae from Miller and Freund provide these moments of *y*:

$$E(y) = ab = \frac{N}{2} \cdot \frac{2\,\sigma_m^2}{N} = \sigma_m^2 \quad \text{and} \quad \sigma_y^2 = a\, b^2 = \frac{N}{2} \cdot \left(\frac{2\,\sigma_m^2}{N}\right)^2 = \frac{2\,\sigma_m^4}{N}.$$

In general, the Gamma distribution does not have a closed-form expression for its cumulative density function, but can be readily evaluated numerically by commonly available software. However, if *N* is even-valued, its CDF for *y* can be written as (Leon-Garcia, 1994):

$$P_{y\leq}(Y) = 1 - \sum_{k=0}^{\frac{N}{2}-1} \frac{\left(\dfrac{N}{2\,\sigma_m^2}\right)^k Y^k\, e^{\frac{-Y \cdot N}{2\sigma_m^2}}}{k!}, \quad Y > 0, N \text{ even.}$$

Now, when the muscle is fully at rest, $s = 0$, and $\sigma_m^2 = q^2$; or $\sigma_m = q$. Thus, the PDF for *y* becomes:

$$p_{y,Rest}(Y) = \begin{cases} \dfrac{Y^{\frac{N}{2}-1}\, e^{\frac{-Y \cdot N}{2q^2}}}{\left(q \sqrt{\dfrac{2}{N}}\right)^N \Gamma\left(\dfrac{N}{2}\right)}, & Y > 0 \\ 0, & \text{otherwise} \end{cases} = \text{Gamma}\left(\frac{N}{2}, \frac{2\,q^2}{N}\right).$$

Hence, when computing $\hat{s}_{\mathrm{RMS}}$ during rest contractions, the probability of estimating a zero value (i.e., the probability that the subtraction within the maximizing function will yield a negative value) equals the cumulative density for *y* evaluated at q^2 during the rest condition, or $P_{y\le q^2,Rest}(Y)$. Substituting into the CDF above (for *N* even) using the fact that $\sigma_m^2 = q^2$ at rest gives:

$$P_{y\le q^2,Rest}(Y)\big|_{Y=q^2,\sigma_m^2=q^2} = 1 - \sum_{k=0}^{\frac{N}{2}-1} \frac{\left(\frac{N}{2\,q^2}\right)^k (q^2)^k\, e^{\frac{-q^2\cdot N}{2q^2}}}{k!} = 1 - \sum_{k=0}^{\frac{N}{2}-1} \frac{\left(\frac{N}{2}\right)^k e^{\frac{-N}{2}}}{k!}, \quad Y>0, N \text{ even.}$$

This result shows that the probability of estimating a zero value is *unrelated* to the standard deviation of the noise—it is *only* related to the smoothing window length.

For the Gaussian model and its corresponding RMS processor, the figure below shows the probability of estimating a zero $\hat{s}_{\mathrm{RMS}}$ value during rest as a function of even values of N_{Eq} between 2 and 200. It would appear that this plot is approaching 0.5 as N_{Eq} increases above 200. Over the practical range of N_{Eq}, this probability does not vary appreciably—it remains near 0.5. Thus, at rest, the maximum likelihood estimate only provides an estimate of zero standard deviation about one half of the samples.

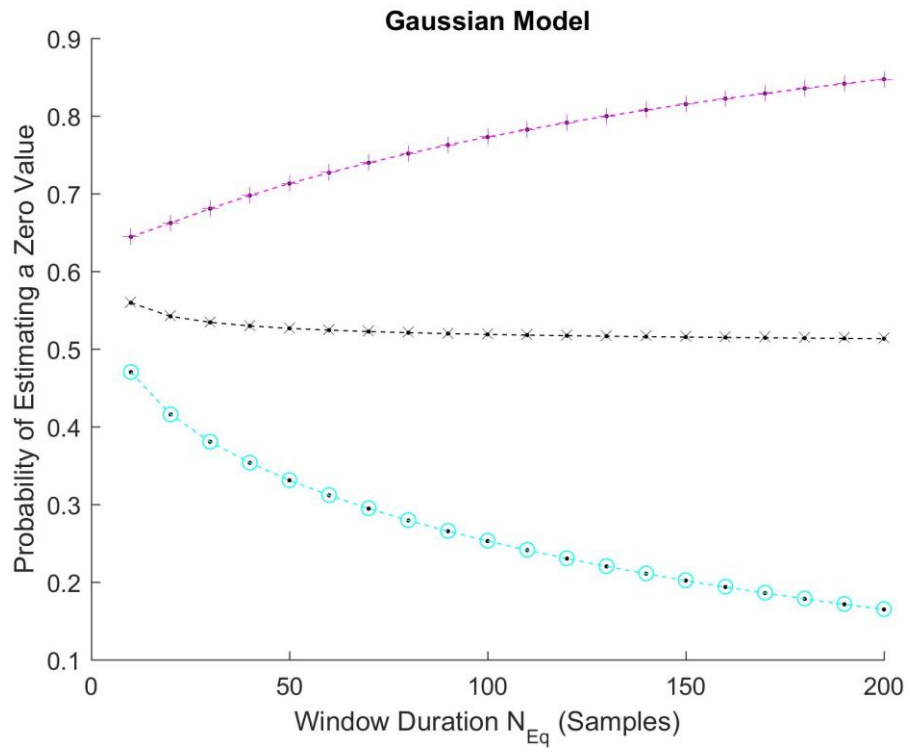

Figure: Plots of theoretical (black ".", for N_{Eq} even-valued) and empirical (black "x") probability of estimating a zero value, as a function of window duration. Empirical results used a noise standard deviation of *q=5*, and 100 million sample duration simulated EMG in MATLAB. Magenta results are for *g*=1.05 (see below) and cyan results are for *g*=0.95.

It may be appropriate to form an estimator that provides an EMGσ estimate of zero with higher probability when the muscle is at rest. For example, myoelectric prosthesis control software very much desires a control signal that equals zero whenever the user's muscles are at rest. Else, the prosthesis will slowly "drift" and change its posture when the user intends the device to remain in its current pose. A reasonable approach to further increase the probability of a zero output during muscle rest is to create the estimate $\hat{s}_{\mathrm{RMS-g}}$ as:

$$\hat{s}_{\mathrm{RMS\_G}} = \sqrt{\max\left[0, \quad \left(\frac{\sum_{n=0}^{N-1} M[n]^2}{N}\right) - g^2 q^2\right]},$$

where $g \geq 0$ is a gain factor that scales the subtraction term. A value of $g>1$ will increase the probability of providing a zero-valued EMGσ estimate. Substituting into the CDF above (for N even) using the fact that $\sigma_m^2 = q^2$ at rest gives:

$$P_{y \leq g^2 q^2, Rest}(Y)\Big|_{Y=g^2 q^2, \sigma_m^2 = q^2} = 1 - \sum_{k=0}^{\frac{N}{2}-1} \frac{\left(\frac{N}{2\,q^2}\right)^k \, (g^2 q^2)^k \, e^{\frac{-g^2 q^2 \cdot N}{2q^2}}}{k!}$$

or

$$P_{y \leq g^2 q^2, Rest}(Y)\Big|_{Y=g^2 q^2, \sigma_m^2 = q^2} = 1 - \sum_{k=0}^{\frac{N}{2}-1} \frac{\left(\frac{N}{2}\right)^k \, g^{2k} \, e^{\frac{-g^2 N}{2}}}{k!}, \quad N \text{ even}.$$

The figure above shows the probability of estimating a zero $\hat{s}_{\mathrm{RMS}}$ value during rest as a function of even values of N between 2 and 200, when g = 0.95, 1 and 1.05. The plots are quite sensitive to this noise gain value. From the plot, it appears that the probability of estimating a zero $\hat{s}_{\mathrm{RMS}}$ value tends towards 0.5 for g=1, towards 1 for g>1, and towards 0 for g<1.

Gaussian Model: MATLAB Validation/Testing

MATLAB was used to test the above Gaussian model formulae. First, one hundred million one hundred (*NN*) independent, zero-mean, unit-variance Gaussian random deviates were arranged into vector $\underline{x}$. One hundred million one hundred independent, zero-mean Gaussian random deviates of standard deviation equal to *q=5* were arranged into vector $\underline{v}$. Vector $\underline{x}$ was initially multiplied by *s=23*, to set the standard deviation of the true EMG signal. The scaled $\underline{x}$ vector was added to the noise vector $\underline{v}$ to form the measured EMG vector $\underline{m}$. Vector $\underline{m}$ was then squared and moving average filtered using a window length of *N=100*. The first *N=100* samples in this result were deleted (to remove the filter startup transient), forming the random vector $\underline{y}$, which should have the PDF $p_y(Y)$ described in this section. A histogram estimate of the PDF of *y* was generated from vector $\underline{y}$ using 101 bins (shown in cyan below)

and compared to the $p_y(Y)$ equation (i.e., theory) derived herein (shown as magenta circles in the figure below) and to the MATLAB function that computes the PDF for a Gamma density with the *a* and *b* parameters as given above (black "x"s). The different techniques compare well. Also shown is the value of $p_{y\leq}(q^2)$ value computed using the MATLAB Gamma CDF function as well as the fraction of $\underline{y}$ values that were less than q^2. Again, these values are equivalent, as expected.

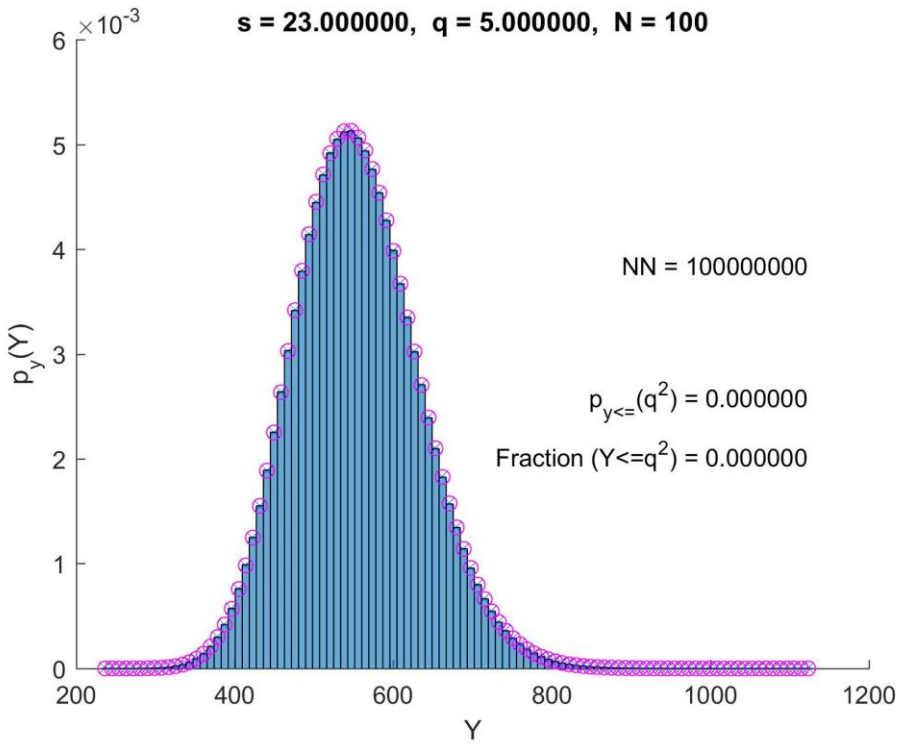

Figure: Shows histogram estimate of PDF (cyan), theoretic estimate of PDF based on the analysis of this section (magenta circles) and theoretic Gamma PDF function of MATLAB (black "x"s). Parameters are: *s* = 23, *q* = 5, *N* = 100 and *NN* = 10,000,000.

Second, a rest contraction was simulated by setting *s=0* and re-computing all results (i.e., using a new instance of random vectors for $\underline{x}$ and $\underline{v}$). That result is shown below. All results were consistent with theory, showing that, at rest, 51.99% of the RMS values are lower than the noise floor.

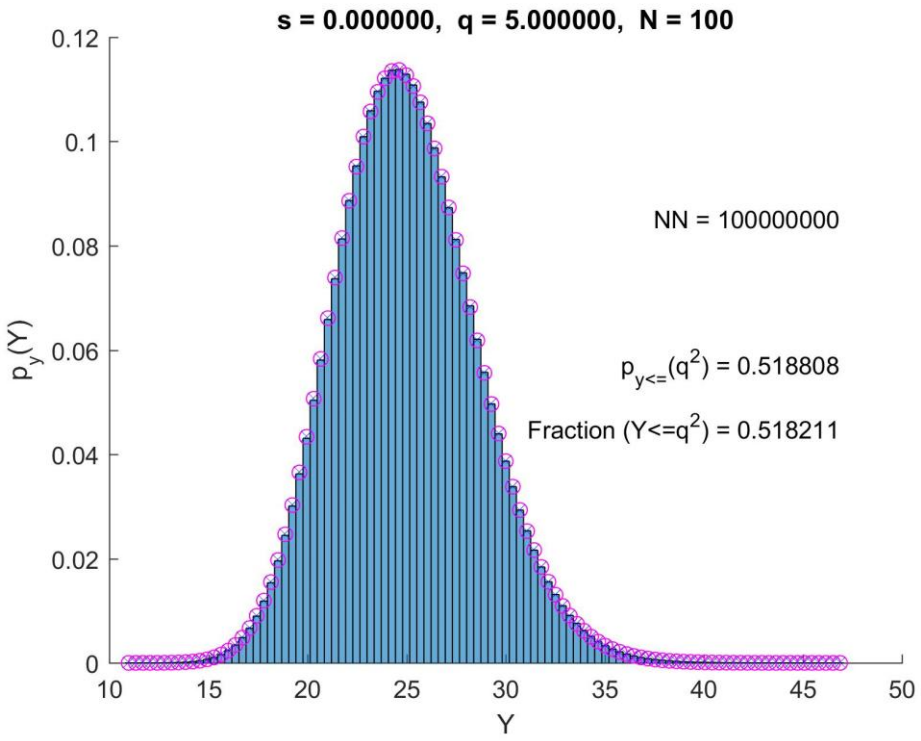

Figure: Shows histogram estimate of PDF (cyan), theoretic estimate of PDF based on the analysis of this section (magenta circles) and theoretic Gamma PDF function of MATLAB (black "x"s). Parameters are: *s* = 0, *q* = 5, *N* = 100 and *NN* = 10,000,000.

Third, another rest contraction was simulated by setting *s=0*, but now also altering the noise intensity be setting the standard deviation of the noise to *q=47*. All results were re-computed using a new instance of random vectors for $\underline{x}$ and $\underline{v}$. That result is shown below. Again, all results were consistent with theory, showing that, at rest, 51.99% of the RMS values are lower than the noise floor.

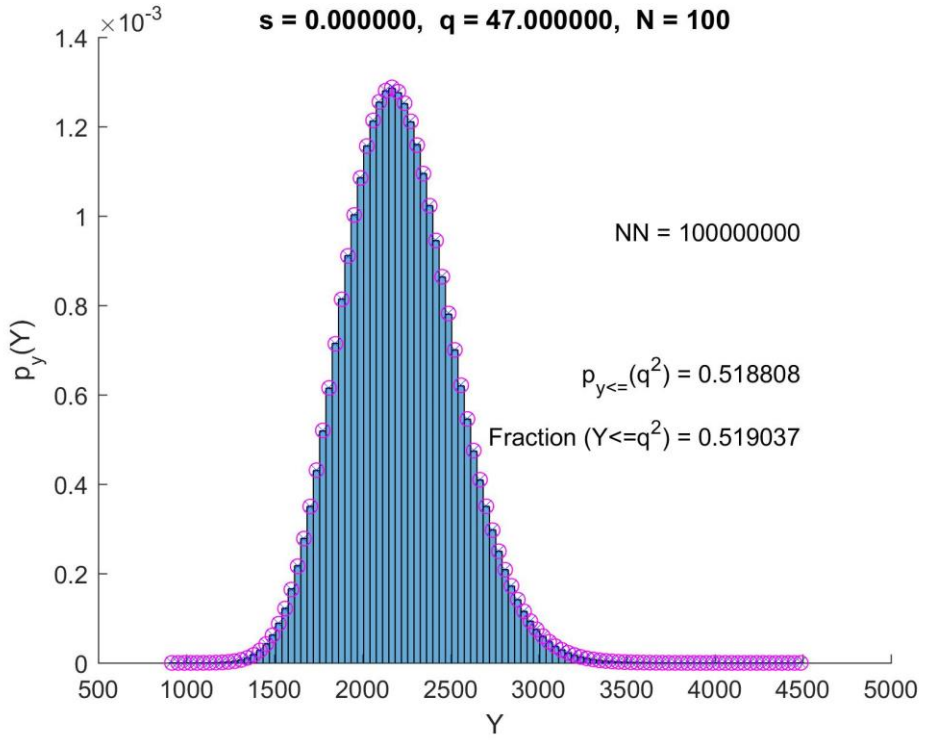

Figure: Shows histogram estimate of PDF (cyan), theoretic estimate of PDF based on the analysis of this section (magenta circles) and theoretic Gamma PDF function of MATLAB (black "x"s). Parameters are: *s* = 0, *q* = 47, *N* = 100 and *NN* = 10,000,000.

Fourth, another rest contraction was simulated by setting *s=0*, returning the noise intensity to *q=5*, but setting the smoothing window duration to *N=200*. All results were re-computed using a new instance of random vectors for $\underline{x}$ and $\underline{v}$. That result is shown below. Again, all results were consistent with theory, showing that, at rest, 51.39% of the RMS values are lower than the noise floor.

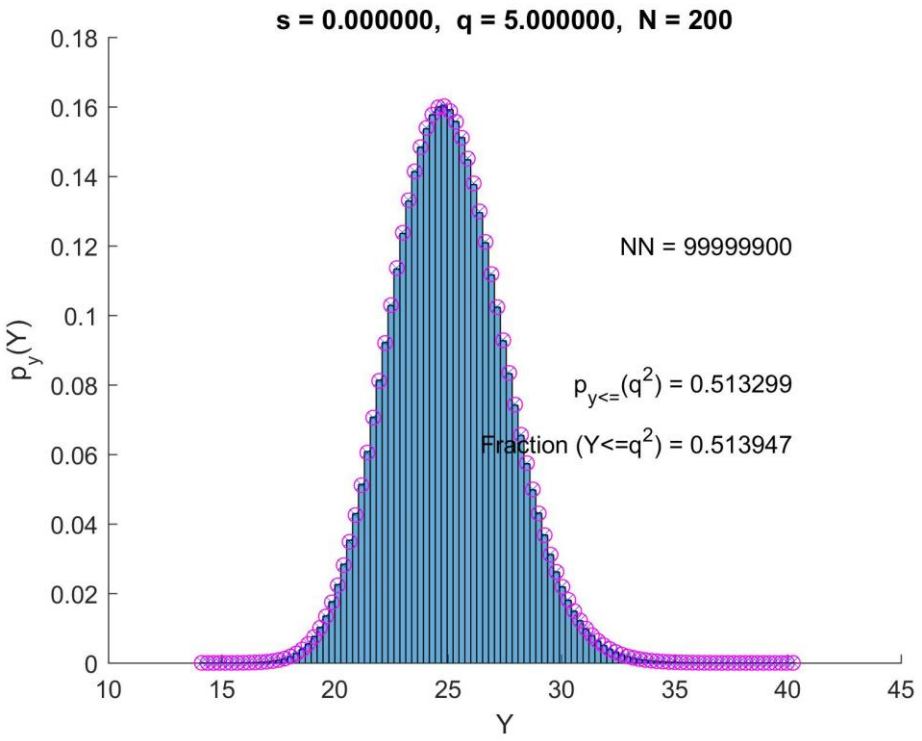

Figure: Shows histogram estimate of PDF (cyan), theoretic estimate of PDF based on the analysis of this section (magenta circles) and theoretic Gamma PDF function of MATLAB (black "x"s). Parameters are: *s* = 0, *q* = 5, *N* = 200 and *NN* = 10,000,000.

Derived Density: Absolute Value of the Laplacian Density

A zero mean Laplacian random variable, *x*, has the probability density function (PDF) (Drake, 1967):

$$p_x(X) = \frac{\sqrt{2}}{2\,\sigma}\, e^{\frac{-\sqrt{2}}{\sigma}|X|}, \quad -\infty \le X \le \infty$$

where σ is the standard deviation. Form random variable *y* as: $y = |x|$. Because of the symmetry about the *x*-axis exhibited by the Laplacian density, the cumulative density function (CDF) for *y* can be written as:

$$P_{y\le}(Y) = \begin{cases} \int_{X=-Y}^{Y} p_x(X)\, dX\,, & Y > 0 \\ 0, & \text{otherwise.} \end{cases}.$$

Substituting the Laplacian density into the integral:

$$P_{y\le}(Y) = \int_{X=-Y}^{Y} \frac{\sqrt{2}}{2\,\sigma}\, e^{\frac{-\sqrt{2}}{\sigma}|X|}\, dX = \frac{\sqrt{2}}{2\,\sigma}\left[\int_{X=-Y}^{0} e^{\frac{\sqrt{2}}{\sigma}X}\, dX + \int_{X=0}^{Y} e^{\frac{-\sqrt{2}}{\sigma}X}\, dX\right]$$

$$= \frac{\sqrt{2}}{2\,\sigma}\left[\frac{e^{\frac{\sqrt{2}}{\sigma}X}}{\frac{\sqrt{2}}{\sigma}}\Bigg|_{X=-Y}^{0} + \frac{e^{\frac{-\sqrt{2}}{\sigma}X}}{\frac{-\sqrt{2}}{\sigma}}\Bigg|_{X=0}^{Y}\right] = \frac{1}{2}\left[e^{\frac{\sqrt{2}}{\sigma}X}\Big|_{X=-Y}^{0} - e^{\frac{-\sqrt{2}}{\sigma}X}\Big|_{X=0}^{Y}\right]$$

$$= \frac{\left(e^{\frac{\sqrt{2}}{\sigma}\cdot 0} - e^{\frac{\sqrt{2}}{\sigma}(-Y)}\right) - \left(e^{\frac{-\sqrt{2}}{\sigma}Y} - e^{\frac{-\sqrt{2}}{\sigma}\cdot 0}\right)}{2} = \frac{1 - e^{\frac{-\sqrt{2}}{\sigma}Y} - e^{\frac{-\sqrt{2}}{\sigma}Y} + 1}{2}$$

$$P_{y\leq}(Y) = \begin{cases} 1 - e^{\frac{-\sqrt{2}}{\sigma}Y}, & Y > 0 \\ 0, & \text{otherwise.} \end{cases}$$

To determine the PDF for *y*, we differentiate this CDF with respect to *Y*:

$$p_y(Y) = \frac{d\,P_{y\leq}(Y)}{dY} = \frac{d\left(1 - e^{\frac{-\sqrt{2}}{\sigma}Y}\right)}{dY} = -\frac{-\sqrt{2}}{\sigma}\,e^{\frac{-\sqrt{2}}{\sigma}Y}$$

$$p_y(Y) = \begin{cases} \frac{\sqrt{2}}{\sigma}\,e^{\frac{-\sqrt{2}}{\sigma}Y}, & Y > 0 \\ 0, & \text{otherwise.} \end{cases}$$

This resulting PDF is exponential, with expected value: $E(y) = \frac{\sigma}{\sqrt{2}}$ (Drake, 1967).

Derived Density: Square of the Erlang Density

An Erlang random variable, *x*, with parameter *N* has the PDF (Drake, 1967):

$$p_x(X) = \begin{cases} \frac{a^N\,X^{N-1}\,e^{-aX}}{(N-1)!} & X > 0,\ a > 0 \\ 0, & \text{otherwise,} \end{cases}$$

where $E(x) = \frac{N}{a}$, $\sigma_x = \frac{\sqrt{N}}{a}$ and *N* is an integer. Form random variable *y* as: $y = x^2$. The CDF for *y* can be found as:

$$P_{y\leq}(Y) = \begin{cases} \int_{X=0}^{\sqrt{Y}} p_x(X)\,dX\,, & Y > 0 \\ 0, & \text{otherwise.} \end{cases}$$

Substituting the *N*-Erlang density into the integral:

$$P_{y\leq}(Y) = \int_{X=0}^{\sqrt{Y}} \frac{a^N\,X^{N-1}\,e^{-aX}}{(N-1)!}\,dX = \frac{a^N}{(N-1)!}\int_{X=0}^{\sqrt{Y}} X^{N-1}\,e^{-aX}\,dX.$$

For *N* an integer, Gradshteyn and Ryzik (Gradshteyn & Ryzhik, 1980) solve this integral using successive stages of integration by parts, giving:

$$P_{y\leq}(Y) = \frac{a^N}{(N-1)!}\left\{e^{-aX}\left[\frac{X^{N-1}}{-a} + \sum_{k=1}^{N-1}(-1)^k\,\frac{(N-1)(N-2)\cdots(N-k)}{(-a)^{k+1}}\,X^{N-1-k}\right]\right\}\Bigg|_{X=0}^{\sqrt{Y}}.$$

Note that for a>0, $\frac{(-1)^k}{(-a)^{k+1}} = \frac{-1}{a^{k+1}}$. Also note that: $(N-1)(N-2)\cdots(N-k) = \frac{(N-1)!}{(N-1-k)!}$. Thus,

$$P_{y\leq}(Y) = \frac{-(a^N)}{(N-1)!}\left\{e^{-aX}\left[\frac{X^{N-1}}{a} + \sum_{k=1}^{N-1}\frac{(N-1)!}{(N-1-k)!\ a^{k+1}}\ X^{N-1-k}\right]\right\}\Bigg|_{X=0}^{\sqrt{Y}}.$$

Evaluating the limits of this definite integral:

$$P_{y\leq}(Y) = \frac{-(a^N)}{(N-1)!}\left\{e^{-a\sqrt{Y}}\left[\frac{\sqrt{Y}^{N-1}}{a} + \sum_{k=1}^{N-1}\frac{(N-1)!}{(N-1-k)!\ a^{k+1}}\ \sqrt{Y}^{N-1-k}\right]\right.$$
$$\left. - e^{-a\cdot 0}\left[\frac{0^{N-1}}{a} + \sum_{k=1}^{N-1}\frac{(N-1)!}{(N-1-k)!\ a^{k+1}}\ 0^{N-1-k}\right]\right\}.$$

Several of the terms involving the evaluation at X=0 can be simplified as:

- $e^{-a\cdot 0} = 1,\ \text{for } a > 0;$
- $\frac{0^{N-1}}{a} = 0,\ \text{for an integer } N > 1;$
- $0^{N-1-k} = 0$ for all terms in the sum except for the final term when $k = N-1$. At this term, $0^{N-1-k}|_{k=N-1} = 0^{N-1-(N-1)} = 0^0 = 1$. Hence, only the final term in the sum is non-zero and the entire sum simplifies to:

$$\sum_{k=1}^{N-1}\frac{(N-1)!}{(N-1-k)!\ a^{k+1}}\ 0^{N-1-k} = \frac{(N-1)!}{(N-1-k)!\ a^{k+1}}\ 0^{N-1-k}\Bigg|_{k=N-1} = \frac{(N-1)!}{0!\ a^N}$$
$$= \frac{(N-1)!}{a^N}.$$

Incorporating each of these simplification into the equation for $P_{y\leq}(Y)$ gives;

$$P_{y\leq}(Y) = \frac{-(a^N)}{(N-1)!}\left\{e^{-a\sqrt{Y}}\left[\frac{\sqrt{Y}^{N-1}}{a} + \sum_{k=1}^{N-1}\frac{(N-1)!}{(N-1-k)!\ a^{k+1}}\ \sqrt{Y}^{N-1-k}\right] - \frac{(N-1)!}{a^N}\right\},$$
$$= \frac{a^N}{(N-1)!}\left\{\frac{(N-1)!}{a^N} - e^{-a\sqrt{Y}}\left[\frac{Y^{\frac{N-1}{2}}}{a} + \sum_{k=1}^{N-1}\frac{(N-1)!}{(N-1-k)!\ a^{k+1}}\ Y^{\frac{N-1-k}{2}}\right]\right\},$$

or

$$P_{y\leq}(Y) = \begin{cases} 1 - e^{-a\sqrt{Y}}\left[\dfrac{a^{N-1}\ Y^{\frac{N-1}{2}}}{(N-1)!} + \displaystyle\sum_{k=1}^{N-1}\frac{a^{N-k-1}}{(N-1-k)!}\ Y^{\frac{N-1-k}{2}}\right] & Y > 0 \\ 0, & \text{otherwise.} \end{cases}$$

To determine the PDF for y, we differentiate this CDF with respect to Y:

$$p_y(Y) = \frac{d\ P_{y\leq}(Y)}{dY} = \frac{d\left(1 - e^{-aY^{\frac{1}{2}}}\left[\frac{a^{N-1}\ Y^{\frac{N-1}{2}}}{(N-1)!} + \sum_{k=1}^{N-1}\frac{a^{N-k-1}}{(N-1-k)!}\ Y^{\frac{N-1-k}{2}}\right]\right)}{dY}$$

$$= -e^{-aY^{\frac{1}{2}}} \cdot \frac{d\left(\frac{a^{N-1}\,Y^{\frac{N-1}{2}}}{(N-1)!} + \sum_{k=1}^{N-1} \frac{a^{N-k-1}}{(N-1-k)!}\,Y^{\frac{N-1-k}{2}}\right)}{dY} + \frac{d\left(-e^{-aY^{\frac{1}{2}}}\right)}{dY}$$

$$\cdot \left(\frac{a^{N-1}\,Y^{\frac{N-1}{2}}}{(N-1)!} + \sum_{k=1}^{N-1} \frac{a^{N-k-1}}{(N-1-k)!}\,Y^{\frac{N-1-k}{2}}\right)$$

$$p_y(Y) = -e^{-aY^{\frac{1}{2}}} \cdot \left(\frac{a^{N-1}}{(N-1)!} \cdot \frac{(N-1)\,Y^{\frac{N-3}{2}}}{2} + \sum_{k=1}^{N-1} \frac{a^{N-k-1}}{(N-1-k)!} \cdot \frac{(N-1-k)\,Y^{\frac{N-3-k}{2}}}{2}\right)$$

$$- \left(\frac{-a\,e^{-aY^{\frac{1}{2}}}}{2\,Y^{\frac{1}{2}}}\right) \cdot \left(\frac{a^{N-1}\,Y^{\frac{N-1}{2}}}{(N-1)!} + \sum_{k=1}^{N-1} \frac{a^{N-k-1}\,Y^{\frac{N-1-k}{2}}}{(N-1-k)!}\right)$$

When $k = N-1$ in the first sum, the summed term simplifies to:

$$\frac{a^{N-k-1}}{(N-1-k)!} \cdot \frac{(N-1-k)\,Y^{\frac{N-3-k}{2}}}{2}\Bigg|_{k=N-1} = \frac{a^{N-(N-1)-1}}{\big(N-1-(N-1)\big)!} \cdot \frac{\big(N-1-(N-1)\big)\,Y^{\frac{N-3-(N-1)}{2}}}{2}$$

$$= \frac{a^0}{(0)!} \cdot \frac{(0)\,Y^{\frac{-2}{2}}}{2} = \frac{1}{1} \cdot \frac{(0)\,Y^{-1}}{2} = \frac{0}{2\,Y} = 0.$$

Thus, this final term in the sum is always zero. This term can be removed from the sum, such that the sum ends at index $k = N-2$. Incorporating this change, switching the order of the two major terms and simplifying/combining gives:

$$p_y(Y) = \left(\frac{e^{-aY^{\frac{1}{2}}}}{2}\right) \cdot \left(\frac{a^N\,Y^{\frac{N-2}{2}}}{(N-1)!} + \sum_{k=1}^{N-1} \frac{a^{N-k}\,Y^{\frac{N-2-k}{2}}}{(N-1-k)!}\right) - \left(\frac{e^{-aY^{\frac{1}{2}}}}{2}\right)$$

$$\cdot \left(\frac{a^{N-1}\,Y^{\frac{N-3}{2}}}{(N-2)!} + \sum_{k=1}^{N-2} \frac{a^{N-k-1}\,Y^{\frac{N-3-k}{2}}}{(N-2-k)!}\right)$$

$$p_y(Y) =$$

$$\begin{cases} \dfrac{a^N\,Y^{\frac{N-2}{2}}\,e^{-aY^{\frac{1}{2}}}}{2} \cdot \left(\dfrac{1}{(N-1)!} + \displaystyle\sum_{k=1}^{N-1} \frac{a^{-k}\,Y^{\frac{-k}{2}}}{(N-1-k)!} - \frac{a^{-1}\,Y^{\frac{-1}{2}}}{(N-2)!} - \sum_{k=1}^{N-2} \frac{a^{-k-1}\,Y^{\frac{-1-k}{2}}}{(N-2-k)!}\right), & Y > 0 \\ 0, & \text{otherwise.} \end{cases}$$

Derived Density: y_{2g} is the Square Root of y_{1g}, Gaussian Model

The maximum likelihood estimate for the Gaussian case is formed as

$$y_{2g} = \sqrt{y_{1g}},$$

where

$$y_{1g} = \max\left[0, \quad \left(\frac{\sum_{n=0}^{N-1} M[n]^2}{N}\right) - g^2 q^2\right],$$

and is has already been shown that

$$p_{y_{1G}}(Y_{1G}) = \begin{cases} 0, & Y_{1G} < 0 \\ \left[1 - \sum_{k=0}^{\frac{N}{2}-1} \frac{\left(\frac{N}{2\,(s^2+q^2)}\right)^k (g^2q^2)^k\, e^{\frac{-(g^2q^2)\cdot N}{2\,(s^2+q^2)}}}{k!}\right]\delta(Y_{1G}), & Y_{1G} = 0, N \text{ even} \\ \dfrac{(Y_{1G} + g^2q^2)^{\frac{N}{2}-1}\, e^{\frac{-(Y_{1G}+g^2q^2)\cdot N}{2\,(s^2+q^2)}}}{\left(\sqrt{\frac{2\,(s^2+q^2)}{N}}\right)^N \Gamma\left(\frac{N}{2}\right)}, & Y_{1G} > 0, N \text{ even.} \end{cases}$$

Cumulative Density Function

We wish to determine the CDF for y_{2g}, which is the probability $P_{y_{2g}\leq}(Y_{2G})$.

- Case 1: $Y_{2G} < 0$:
  - The CDF for y_{2g} is zero for $Y_{2G} < 0$, since $p_{y_{1G}}(Y_{1G}) = 0$ for $Y_{1G} < 0$, and $\sqrt{0} = 0$. No probability is accumulated.
- Case 2: $Y_{2G} = 0$:
  - Since the square root of zero equals zero, the impulsive probability associated with the value zero is not altered by the square root function. Thus, the same impulse of probability will remain associated with this location. Since there is no accumulated probability prior to $Y_{2G} = 0$ (scanning back to $-\infty$) and the CDF integrates this impulsive probability at $Y_{2G} = 0$,

$$P_{y_{2G}\leq}(Y_{2G})$$

$$= \left[1 - \sum_{k=0}^{\frac{N}{2}-1} \frac{\left(\frac{N}{2\,(s^2+q^2)}\right)^k (g^2q^2)^k\, e^{\frac{-(g^2q^2)\cdot N}{2\,(s^2+q^2)}}}{k!}\right]\mu(Y_{2G}) \equiv P_{y_{2G}\leq}(Y_{2G} = 0), \quad N \text{ even},$$

where $\mu(Y_{2G}) = \begin{cases} 0, & Y_{2G} < 0 \\ 1, & Y_{2G} \geq 0 \end{cases}$ is the unit step function.

- Case 3: $Y_{2G} > 0$:
  - In this case, the CDF for y_{2G} will accumulate the probability associated with $Y_{2G} = 0$ as well as the probability associated with $Y_{2G} > 0^+$:

$$P_{y_{2G\leq}}(Y_{2G}) = P_{y_{2G\leq}}(Y_{2G}=0) + \int_{Y_{1G}=0}^{Y_{2G}^2} p_{y_{1G}}(Y_{1G})\, dY_{1G}.$$

Focusing on the integral:

$$\int_{Y_{1G}=0}^{Y_{2G}^2} p_{y_{1G}}(Y_{1G})\, dY_{1G} = \int_{Y_{1G}=0}^{Y_{2G}^2} \frac{(Y_{1G}+g^2q^2)^{\frac{N}{2}-1}\, e^{\frac{-(Y_{1G}+g^2q^2)\cdot N}{2\,(s^2+q^2)}}}{\left(\sqrt{\frac{2\,(s^2+q^2)}{N}}\right)^N \Gamma\left(\frac{N}{2}\right)}\, dY_{1G}$$

$$= \frac{\int_{Y_{1G}=0}^{Y_{2G}^2} (Y_{1G}+g^2q^2)^{\frac{N}{2}-1}\, e^{\frac{-(Y_{1G}+g^2q^2)\cdot N}{2\,(s^2+q^2)}}\, dY_{1G}}{\left(\sqrt{\frac{2\,(s^2+q^2)}{N}}\right)^N \Gamma\left(\frac{N}{2}\right)}.$$

Since N is even-valued, $\frac{N}{2} \equiv M$ is an integer. Let $a = g^2q^2$ and $b = \frac{N}{2\,(s^2+q^2)} = \frac{M}{(s^2+q^2)}$. The integral becomes:

$$\int_{Y_{1G}=0}^{Y_{2G}^2} p_{y_{1G}}(Y_{1G})\, dY_{1G} = \frac{\int_{Y_{1G}=0}^{Y_{2G}^2} (Y_{1G}+a)^{M-1}\, e^{-b(Y_{1G}+a)}\, dY_{1G}}{\left(\sqrt{\frac{2\,(s^2+q^2)}{N}}\right)^N \Gamma\left(\frac{N}{2}\right)}.$$

Using the on-line Wolfram Alpha web site (2019/04/01), this integral is solved, providing

$$\int_{Y_{1G}=0}^{Y_{2G}^2} p_{y_{1G}}(Y_{1G})\, dY_{1G} = \frac{-(Y_{1G}+a)^M [b(Y_{1G}+a)]^{-M}\, \Gamma_{Inc}[M, b(Y_{1G}+a)]\big|_{Y_{1G}=0}^{Y_{2G}^2}}{\left(\sqrt{\frac{2\,(s^2+q^2)}{N}}\right)^N \Gamma\left(\frac{N}{2}\right)},$$

where $\Gamma_{Inc}(\cdot)$ is the upper incomplete Gamma function, defined as

$$\Gamma_{Up}(\alpha, x) \equiv \int_{t=x}^{\infty} t^{\alpha-1} e^{-t}\, dt.$$

Substituting the definite limits of the integral:

$$\int_{Y_{1G}=0}^{Y_{2G}^2} p_{y_{1G}}(Y_{1G})\, dY_{1G}$$

$$= \frac{-(Y_{2G}^2+a)^M [b(Y_{2G}^2+a)]^{-M}\, \Gamma_{Up}[M, b(Y_{2G}^2+a)] - -(0+a)^M [b(0+a)]^{-M}\, \Gamma_{Up}[M, b(0+a)]}{\left(\sqrt{\frac{2\,(s^2+q^2)}{N}}\right)^N \Gamma\left(\frac{N}{2}\right)}$$

$$= \frac{-(Y_{2G}^2 + a)^M [b(Y_{2G}^2 + a)]^{-M}\ \Gamma_{Up}[M, b(Y_{2G}^2 + a)] + a^M\ (b \cdot a)^{-M}\ \Gamma_{Up}[M, b \cdot a]}{\left(\sqrt{\frac{2\ (s^2 + q^2)}{N}}\right)^N\ \Gamma\left(\frac{N}{2}\right)},$$

$$= \frac{-b^{-M}\ \Gamma_{Up}[M, b(Y_{2G}^2 + a)] + \ b^{-M}\ \Gamma_{Up}[M, b \cdot a]}{\left(\sqrt{\frac{2\ (s^2 + q^2)}{N}}\right)^N\ \Gamma\left(\frac{N}{2}\right)}.$$

From the definitions above,

$$\left(\sqrt{\frac{2\ (s^2 + q^2)}{N}}\right)^N\ \Gamma\left(\frac{N}{2}\right) = \left(\sqrt{b^{-1}}\right)^N\ \Gamma(M) = b^{\frac{-N}{2}}\ \Gamma(M) = b^{-M}\ \Gamma(M).$$

Thus,

$$\int_{Y_{1G}=0}^{Y_{2G}^2} p_{y_{1G}}(Y_{1G})\ dY_{1G} = \frac{-b^{-M}\ \Gamma_{Up}[M, b(Y_{2G}^2 + a)] + \ b^{-M}\ \Gamma_{Up}[M, b \cdot a]}{b^{-M}\ \Gamma(M)},$$

$$= \frac{-\Gamma_{Up}[M, b(Y_{2G}^2 + a)] + \Gamma_{Up}[M, b \cdot a]}{\Gamma(M)}$$

Then, the complete CDF for this case is:

$$P_{y_{2G\leq}}(Y_{2G}) = P_{y_{2G\leq}}(Y_{2G} = 0) + \int_{Y_{1G}=0}^{Y_{2G}^2} p_{y_{1G}}(Y_{1G})\ dY_{1G},$$

$$= \left[1 - \sum_{k=0}^{\frac{N}{2}-1} \frac{\left(\frac{N}{2\ (s^2 + q^2)}\right)^k\ (g^2 q^2)^k\ e^{\frac{-(g^2 q^2)\cdot N}{2\ (s^2 + q^2)}}}{k!}\right] \mu(Y_{2G})$$

$$+ \frac{-\Gamma_{Up}[M, b(Y_{2G}^2 + a)] + \Gamma_{Up}[M, b \cdot a]}{\Gamma(M)}\ \mu(Y_{2G}),$$

or

$$P_{y_{2G\leq}}(Y_{2G}) = \left[1 - \sum_{k=0}^{M-1} \frac{b^k\ a^k\ e^{-a\cdot b}}{k!} + \frac{\Gamma_{Up}[M, b \cdot a] - \Gamma_{Up}[M, b(Y_{2G}^2 + a)]}{\Gamma(M)}\right] \mu(Y_{2G}).$$

Note that Wikipedia (see “Special values” in https://en.wikipedia.org/wiki/Incomplete_gamma_function, accessed 2019/04/03) and

Wolfram MathWorld (http://mathworld.wolfram.com/IncompleteGammaFunction.html, accessed 2019/04/03) claim for α a positive integer,

$$\Gamma_{Up}(\alpha, x) = (\alpha - 1)!\ e^{-x} \sum_{k=0}^{\alpha-1} \frac{x^k}{k!}.$$

Thus, the right-most term in the square brackets above can be written as:

$$\frac{\Gamma_{Up}[M, b \cdot a] - \Gamma_{Up}[M, b(Y_{2G}^2 + a)]}{\Gamma(M)}$$

$$= \frac{(M-1)!\ e^{-b\cdot a} \sum_{k=0}^{M-1} \frac{(b\cdot a)^k}{k!} - (M-1)!\ e^{-\,b\left(Y_{2G}^2+a\right)} \sum_{k=0}^{M-1} \frac{\left(b(Y_{2G}^2 + a)\right)^k}{k!}}{(M-1)!}$$

$$= e^{-b\cdot a} \sum_{k=0}^{M-1} \frac{(b\cdot a)^k}{k!} - e^{-\,ba - bY_{2G}^2} \sum_{k=0}^{M-1} \frac{\left(b(Y_{2G}^2 + a)\right)^k}{k!}$$

$$= e^{-b\cdot a} \left[\sum_{k=0}^{M-1} \frac{(b\cdot a)^k - e^{-bY_{2G}^2} \left(b(Y_{2G}^2 + a)\right)^k}{k!} \right]$$

$$= e^{-b\cdot a} \left[\sum_{k=0}^{M-1} \frac{b^k \left[a^k - e^{-bY_{2G}^2} (Y_{2G}^2 + a)^k\right]}{k!} \right]$$

Re-combining gives the CDF expression:

$$P_{y_{2G\leq}}(Y_{2G}) = \left\{ 1 - \sum_{k=0}^{M-1} \frac{b^k\, a^k\, e^{-a\cdot b}}{k!} + e^{-b\cdot a} \left[\sum_{k=0}^{M-1} \frac{b^k \left[a^k - e^{-bY_{2G}^2} (Y_{2G}^2 + a)^k\right]}{k!} \right] \right\} \mu(Y_{2G}),$$

N even.

Note, however, that the sum on the left side cancels with the first term of the sum on the right side. Thus, the CDF can more simply be written as:

$$P_{y_{2G\leq}}(Y_{2G}) = \left\{ 1 + e^{-b\cdot a} \left[\sum_{k=0}^{M-1} \frac{b^k \left[-e^{-bY_{2G}^2} (Y_{2G}^2 + a)^k\right]}{k!} \right] \right\} \mu(Y_{2G})$$

$$= \left[1 - e^{-b\cdot a} \sum_{k=0}^{M-1} \frac{b^k\, e^{-bY_{2G}^2} (Y_{2G}^2 + a)^k}{k!} \right] \mu(Y_{2G})$$

$$P_{y_{2G\leq}}(Y_{2G}) = \left[1 - e^{-b\cdot\left(Y_{2G}^2+a\right)} \sum_{k=0}^{M-1} \frac{b^k (Y_{2G}^2 + a)^k}{k!} \right] \mu(Y_{2G}), \qquad N \text{ even}$$

with $M = \frac{N}{2}$ an integer, $a = g^2 q^2$, and $b = \frac{N}{2\,(s^2+q^2)} = \frac{M}{(s^2+q^2)}$. Note that this function has a step discontinuity at $Y_{2G} = 0$, which produces an impulse at this location in the corresponding PDF.

Probability Density Function

The PDF $p_{y_{2G}}(Y_{2G})$ is found by differentiating the CDF $P_{y_{2G\leq}}(Y_{2G})$. Note that $P_{y_{2G\leq}}(Y_{2G})$ equals zero for $Y_{2G} < 0$, steps up to the value given by $P_{y_{2G\leq}}(Y_{2G} = 0)$ F at $Y_{2G} = 0$, and then increases smoothly towards a value of one for $Y_{2G} > 0$. Hence:

- Case 1: $Y_{2G} < 0$:
  - The PDF for y_{2g} is zero for $Y_{2G} < 0$, since $P_{y_{2G\leq}}(Y_{2G}) = 0$ for $Y_{2G} < 0$.
- Case 2: $Y_{2G} = 0$:
  - An impulse of probability will exist at this location. We can arrive at this conclusion in two manners. First, random variable y_{1G} has an impulse at $y_{1G} = 0$ and the square root operation does not alter this impulse ($\sqrt{0} = 0$). That is, all values that were zero prior to the square root operation will remain zero, and all values that were greater than zero will remain so. Thus, y_{2G} will have the identical probability impulse at $y_{2G} = 0$ as does y_{1G}. Second, we can differentiate the equation for $P_{y_{2G\leq}}(Y_{2G})$. Since $P_{y_{2G\leq}}(Y_{2G})$ has a step change at zero, this step change height (i.e., the CDF value at $Y_{2G} = 0$) becomes the area of the impulse at $Y_{2G} = 0$. Thus,

$$p_{y_{2G}}(Y_{2G}) = 1 - \sum_{k=0}^{M-1} \frac{b^k\, a^k\, e^{-a\cdot b}}{k!}\ \delta(Y_{2G}).$$

- Case 3: $Y_{2G} > 0$:
  - Ignoring the step change in value at $Y_{2G} = 0$ (it is already accounted for in the prior case), the PDF is found by differentiating the CDF:

$$p_{y_{2G}}(Y_{2G}) = \frac{d\left\{P_{y_{2G\leq}}(Y_{2G})\right\}}{d\, Y_{2G}}$$

$$p_{y_{2G}}(Y_{2G}) = \frac{d\left\{1 - e^{-b\cdot\left(Y_{2G}^2+a\right)}\ \sum_{k=0}^{M-1} \frac{b^k\,(Y_{2G}^2 + a)^k}{k!}\right\}}{d\, Y_{2G}}$$

$$= \frac{d\left\{-e^{-b\cdot\left(Y_{2G}^2+a\right)}\ \sum_{k=0}^{M-1} \frac{b^k\,(Y_{2G}^2 + a)^k}{k!}\right\}}{d\, Y_{2G}}$$

$$= -e^{-b\cdot\left(Y_{2G}^2+a\right)}\ \frac{d\left\{\sum_{k=0}^{M-1} \frac{b^k\,(Y_{2G}^2 + a)^k}{k!}\right\}}{d\, Y_{2G}} + \frac{d\left\{-e^{-b\cdot\left(Y_{2G}^2+a\right)}\right\}}{d\, Y_{2G}} \sum_{k=0}^{M-1} \frac{b^k\,(Y_{2G}^2 + a)^k}{k!}$$

$$= -e^{-b\cdot\left(Y_{2G}^2+a\right)}\ \frac{d\left\{\frac{b^0\,(Y_{2G}^2+a)^0}{0!}+\sum_{k=1}^{M-1}\frac{b^k\,(Y_{2G}^2+a)^k}{k!}\right\}}{d\,Y_{2G}} + \left[2\,b\,Y_{2G}\,e^{-b\cdot\left(Y_{2G}^2+a\right)}\right]\sum_{k=0}^{M-1}\frac{b^k\,(Y_{2G}^2+a)^k}{k!}$$

$$= -e^{-b\cdot\left(Y_{2G}^2+a\right)}\ \frac{d\left\{1+\sum_{k=1}^{M-1}\frac{b^k\,(Y_{2G}^2+a)^k}{k!}\right\}}{d\,Y_{2G}} + \left[2\,b\,Y_{2G}\,e^{-b\cdot\left(Y_{2G}^2+a\right)}\right]\sum_{k=0}^{M-1}\frac{b^k\,(Y_{2G}^2+a)^k}{k!}$$

$$= -e^{-b\cdot\left(Y_{2G}^2+a\right)}\left[\sum_{k=1}^{M-1}\frac{b^k\,k\,(Y_{2G}^2+a)^{k-1}}{k!}\cdot 2\ Y_{2G}\right] + \left[2\,b\,Y_{2G}\,e^{-b\cdot\left(Y_{2G}^2+a\right)}\right]\sum_{k=0}^{M-1}\frac{b^k\,(Y_{2G}^2+a)^k}{k!}$$

$$= -2\ Y_{2G}\,e^{-b\cdot\left(Y_{2G}^2+a\right)}\left\{\left[\sum_{k=1}^{M-1}\frac{b^k\,k\,(Y_{2G}^2+a)^{k-1}}{k!}\right] - b\sum_{k=0}^{M-1}\frac{b^k\,(Y_{2G}^2+a)^k}{k!}\right\}$$

$$= -2\ Y_{2G}\,e^{-b\cdot\left(Y_{2G}^2+a\right)}\left\{\left[\sum_{k=1}^{M-1}\frac{b^k\,k\,(Y_{2G}^2+a)^{k-1}}{k!}\right] - b\left[1+\sum_{k=1}^{M-1}\frac{b^k\,(Y_{2G}^2+a)^k}{k!}\right]\right\}$$

$$= -2\ Y_{2G}\,e^{-b\cdot\left(Y_{2G}^2+a\right)}\left\{-b+\sum_{k=1}^{M-1}\frac{b^k\,k\,(Y_{2G}^2+a)^{k-1}}{k!} - b\sum_{k=1}^{M-1}\frac{b^k\,(Y_{2G}^2+a)^k}{k!}\right\}$$

$$= 2\ Y_{2G}\,e^{-b\cdot\left(Y_{2G}^2+a\right)}\left\{b+\sum_{k=1}^{M-1}\frac{b^k\,[b\,(Y_{2G}^2+a)^k - k\,(Y_{2G}^2+a)^{k-1}]}{k!}\right\}$$

Thus, the full solution for the PDF is:

$$p_{y_{2G}}(Y_{2G}) = \begin{cases} 0, & Y_{2G} < 0 \\ \left[1-\sum_{k=0}^{M-1}\frac{b^k\,a^k\,e^{-a\cdot b}}{k!}\right]\delta(Y_{2G}), & Y_{2G}=0, N \text{ even} \\ 2\,Y_{2G}\,e^{-b\cdot\left(Y_{2G}^2+a\right)}\left\{b+\sum_{k=1}^{M-1}\frac{b^k\,[b\,(Y_{2G}^2+a)^k - k\,(Y_{2G}^2+a)^{k-1}]}{k!}\right\}, & Y_{2G}>0, N \text{ even}, \end{cases}$$

with $M=\frac{N}{2}$ an integer, $a=g^2q^2$, and $b=\frac{N}{2\,(s^2+q^2)}=\frac{M}{(s^2+q^2)}$.

References

Clancy, E. A. (1991). *Stochastic Modeling of the Relationship Between the Surface Electromygram and Muscle Torque.* Ph.D Thesis, Massachusetts Institute of Technology, p. 449–469,

Drake, A. W. (1967). In *Fundamentals of Applied Probability Theory* (pp. 103–107, 273–274). New York: McGraw-Hill Book Company.

Gradshteyn, I. S., & Ryzhik, I. M. (1980). In *Table of Integrals, Series, and Products* (pp. 92). New York: Academic Press, Inc.

Leon-Garcia, A. (1994). In *Probability and Random Processes for Electrical Engineering* (2nd ed., pp. 118). Reading, MA: Addison-Wesley Publishing Company.

Miller, I., & Freund, J. E. (1977). In *Probability and Statistics for Engineers, 2nd edition* (pp. 117–118, 272–275): Prentice-Hall, Inc.

Papoulis, A. (1984). In *Probability, Random Variables, and Stochastic Processes* (pp. 77, 187). New York: McGraw-Hill Book Company.